Assessing the effect of intrinsic and extrinsic stress inducers on myosin VI distribution.

Björk Aston
Sept 2017-Sept 2018
University of Kent (UKC)
Toseland Lab

Abstract:
Overexpression of the unconventional motor protein myosin VI (*MYOVI*) has been seen in aggressive cancer phenotypes. Its ability to interact with numerous intracellular pathways influences downstream targets and promotes cell growth. Recently MYOVI has been found to positively impact the *ER* pathway directly through the estrogen receptor. Activation of this receptor results in downstream signaling via estrogen responsive elements (EREs) to regulate transcription of a vast plethora of genes including *P53*. Furthermore interactions with Dab2, which binds to the WWY motif located in MYOVI's cargo binding domain, hinder MYOVI's functionality in transcription factories within the nucleus, hence negatively impacting ER-driven gene expression. To assess, in the context of cancer, what is regulating MYOVI distribution within cells we performed experiments to compare the effect of intrinsic protein interactions, using the *ESR1-DAB2* fusion gene isolated from an endocrine therapy resistant metastatic breast cancer (MBC) patient treated with tamoxifen, to extrinsic environmental changes, in this case hypoxia. While the majority of breast cancers in patients are ER-positive (ER+), and hence respond to endocrine therapy, acquired resistance to therapy is a big problem. Determining the localization and interactions in vitro of ESR1-DAB2 and elucidating its association with MYOVI could highlight novel therapeutic targets in MBC. Hypoxia characteristics are found in many tumours and are associated with a poor prognosis. Low oxygen levels alter the transcriptome of cells drastically, typically favouring pathways that upregulate vascular endothelial growth factor (*VEGF*) encouraging angiogenesis to relieve the hypoxic stress. Microscopy revealed that the effect of *ESR1-DAB2* varies between MCF7 and HeLa cell lines and MYOVI distribution can be compared, with the plasmid exhibiting higher toxicity in HeLa potentially due to the loss of *ER* in this cell line. While hypoxia did not result in increased expression levels of MYOVI, the distribution was altered depending on the duration of hypoxia. The data presented in this thesis is not conclusive but lays a foundation to build upon in future work and contributes to the growing collection of roles MYOVI has been found to play.

Contents:

Acronyms

ER- Estrogen Receptor

LBD- ligand binding domain

MBC- metastatic breast cancer

DAB2- disabled-2

MYOVI- myosi VI

RNAPII- RNA Polymerase II

ROCK-2- Rho-associated coiled-coil containing kinase 2

PI3K- phosphoinositide 3-kinase

JNK- c-Jun N-terminal kinase

ERK1/2- extracellular-signal-regulated kinase

NFkB- nuclear factor kappa-light-chain-enhancer of activated B cells

HER2- human epidermal growth factor receptor 2

MAPK- mitogen-activated protein kinase

MTA1- metastasis-associated protein 1

VEGF- vascular endothelial growth factor

AKT- (PKB) protein kinase B

CREB- cAMP response element binding protein

DNA- deoxyribonucleic acid

GFP- green fluorescence protein

RFP- red fluorescence protein

PKA- protein kinase A

PAK1- p21 activated kinase 1

SP-1- specificity protein 1

AP-1- activator protein 1

TGF-β – Tumour growth factor β

Wnt- wingless-related integration site

ERE- estrogen responsive element

E2- estrogen

EGFR – epidermal growth factor receptor

RTK- receptor tyrosine kinase

HIF-α- hypoxia inducible factor α

List of Figures:

1.0: Introduction:

The actin-myosin (actomyosin) network functions within all types of cells in order to regulate a large plethora of cellular functions. The intracellular actin population can be categorized into monomeric and filamentous states, G-actin and F-actin respectively (1). Globular actin monomers, in the presence of ATP, are able to form a filament, where the plus end exhibits faster additions than the minus end. Filaments are enriched in muscle cells, due to their function as contractile fibers in sarcomeres alongside myosin II, but are also found in all cells owing to their key role as part of the cytoskeleton. In eukaryotic cells the cytoskeleton is integral for phagocytosis, maintainence of essential permanent structures for specific cells (such as microvilli in brush-border cells), ensures intra-cellular compartmental integrity, effective transportation of intracellular proteins and functions critically in chromosome segregation and cell division. All forms of myosin exhibit highly conserved actin and ATP-binding sites within the motor head domain. This enables their dynamic ATP-dependent interaction with actin, resulting in a range of cellular functions, including transportation of cargo proteins across cells to the correct cellular compartment (2). Myosin activation mediates endocytosis and exocytosis, as well as cell proliferation, adhesion and migration through the actin cytoskeleton. Tumours exhibit altered mechanical function of the myosins in order to favor proliferation and dissemination by manipulating the actomyosin network (3).

The arrangement of the actomyosin cytoskeleton is mediated by extracellular signals transduced by the Rho protein family. *RHO*, *RAC* and *CDC-42* are not frequently seen to be mutated in cancer, but misregulation of this pathway results in the observed overexpression of *RAC1*, *RHOA* and *CDC-42* in cancer (breast cancer specifically), resulting in tumorigenesis and metastasis due to their influence (4,5). In light of this it is important to not only look into myosin's expression and distribution but also observe how this network is altered by stressors typically observed in more aggressive tumours. This study focuses on observing the effect of protein and environmental stressors on Myosin VI within cancer cells in order to gain further understanding of the pathways at work in aggressive phenotypes.

1.1: Metastatic breast cancers

Breast cancer has been predicted to affect 1 in 8 women during their lifetime and currently makes up to ~30% of cancers found in women. Western Europe has the highest numbers of prevalence for this disease and hence progress has been made to attempt to identify risk factors and reduce the mortality. This has mainly been achieved through screening schemes which use X-rays to detect abnormalities in the breast tissue, allowing early stage breast cancers in women across the world to be identified, and has resulted in an impressive drop in mortality rates for this type of cancer (6). Genomic studies from these patients function not only as a diagnostic tool, but has allowed further investigation into contributing risk factors, highlighting prevalent cancer associated mutations, such as the inactivation of *TP53* via missense mutations and more rare mutations like the *ESR1-DAB2* fusion (92). While early detection is key for a better prognosis, it is also integral to consider the nature of the cancer and its characteristics in order to ascertain the most effective route of therapy for each individual patient (7). Endocrine therapies have successfully treated breast cancers that are Estrogen receptor positive (ER+), as 70% of patients fall into this category. Unforeseeably, 25% of these patients, with metastatic breast cancer (MBC), are then seen to develop resistance to these methods of treatment.

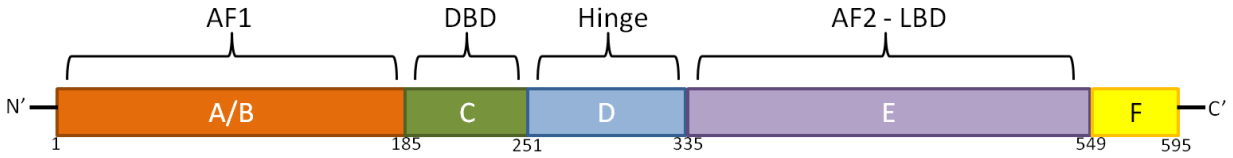

Diagram 1: A cartoon displaying the structure of *ERα*. Domain A/B is the N terminal ligand-independent AF-1 and is followed by the DNA binding domain (B) which also facilitates dimerization. These domains share 97% homology with ERβ and are succeeded by a hinge region (D) which is not conserved between the two types of ER. Section E contains the Ligand binding domain and the C-terminal ligand-dependent AF-2 which is only 55% homologous to that observed in ERβ and F is the c-terminal domain.

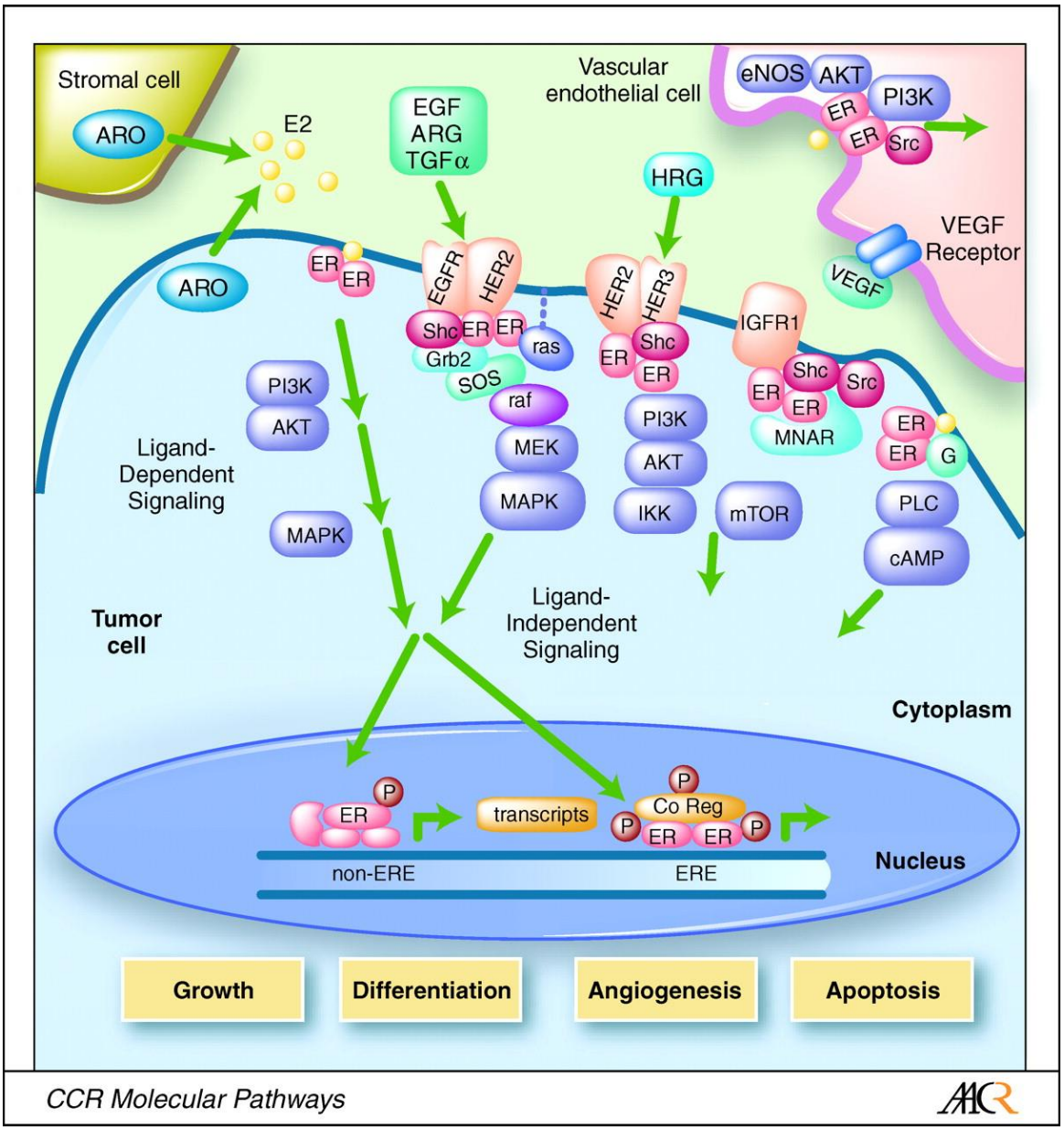

Diagram 2: Estrogen signaling in breast cancer: Membrane bound receptors EGFR and HER2 transduce a signaling cascade through the action of RTK's that activate cytoplasmic proteins by phosphorylation. This can act in a ligand-dependent and ligand-independent manner. Estrogen facilitates the dimerisation of ERα on the membrane, which can then move into the nucleus where the dimer binds directly to ERE's in genes involved in regulating growth, differentiation, angiogensis and apoptosis. (Diagram taken from: Pietras, R.J., Marquez-Garban, D.., (2007) Membrane-Associated Estrogen Receptor signaling pathways in human cancers, Clinical cancer research, DOI: 10.1158/1078-0432.CCR-07-1373)

The mechanism by which acquired resistance to selective estrogen modulators (such as Tamoxifen), selective ER degraders (such as Fulvestrant) and aromatase inhibitors or ovarian suppression techniques is unknown but recent analysis of the Estrogen receptor gene (*ESR1*) has revealed common genetic mutations across MBC patients that may facilitate resistance.

The alterations are commonly point mutations/single nucleotide variants (SNVs) in the codons coding Tyr537 and Asp538 residues within the ligand binding domain (LBD) as seen in diagram 1, altering the structure of the C terminal helix 12 in the receptor, shifting the conformation of the ER, hereby facilitating activation of ER-dependent transcription and proliferation as demonstrated in Diagram 2(8). Further studies of patients with endocrine therapy resistant MBC revealed the presence of an *ESR1-Disabled 2 (DAB2)* fusion gene in an individual treated with Tamoxifen ([29]).

1.2: Myosin VI (MYOVI)

This 150kDa unconventional myosin is present in both the cytoplasm and nucleus of mammalian cells. MYOVI performs its functions as a monomer or a dimer and has the unique ability to move towards the negative end of actin filaments.

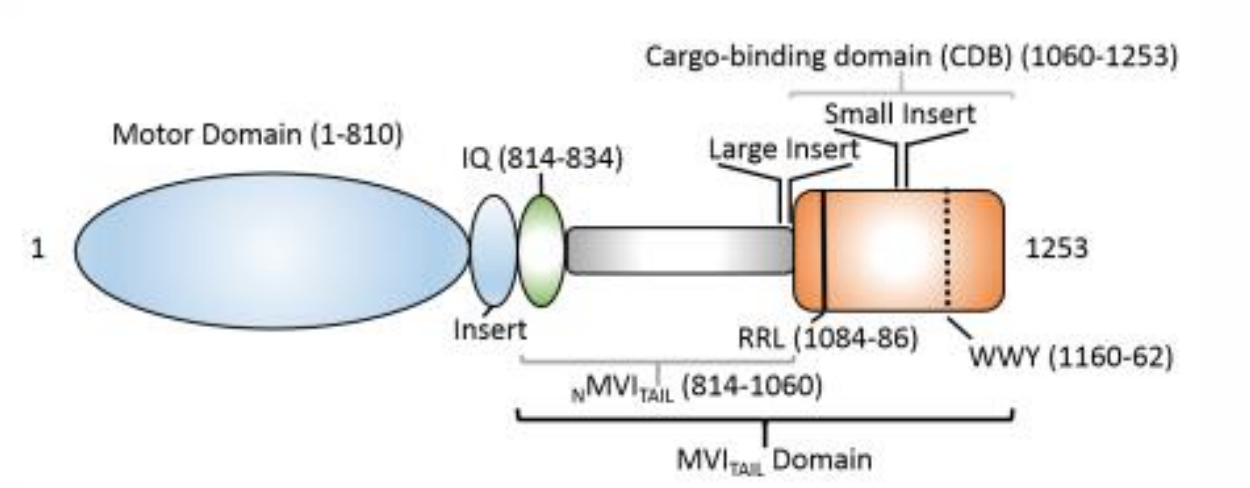

Diagram 3: A cartoon of the motor protein Myosin VI, depicting the catalytic motor head domain and tail region containing the CBD. Isoform sequences are indicated in the tail region where these inserts result in the splice variants large insert (LI), Small insert (SI), LI+SI and the non-insert which contains neither amino acid sequences.

Structurally, it consists of the catalytic head domain, the converter, the medial tail, the proximal tail and the globular cargo binding domain (CBD) as shown below in the cartoon. It exists as four isoforms, a large insert (LI), small insert (SI), large and small insert (LI+SI) and a non-insert (NI), which result from alternate splicing in the tail region. The ratio of isoforms is seen to vary between cell types where each isoform has a niche selection of binding partners in line with the protein's intracellular function.

For instance the large insert (LI) is typically 21-31 amino acids and its presence results in the localization of MYOVI to the apical surfaces enabling it to perform endocytic functions in conjunction with clathrin-pits. The non-insert (NI) has been found to be localized to the trans-side of the Golgi, where it is active in sorting pathways (9).

The CBD contains two motifs which mediate the interaction of MYOVI with its various binding partners. This allows MYOVI to perform a wide range of functions such as functioning as a structural scaffold in the inner ear by localization on filidopia, motor function by dimerisation exhibiting movement towards the negative end of actin filaments(10)in the endocytic pathway and functions in cell migration. The WWY motif is a highly conserved sequence facilitating the binding of MYOVI to DAB2, a single amino acid change in this motif results in the eradication of this binding site. A second RRL binding motif interacts with the glucose transporter binding protein and is also highly conserved (11).

In addition to its cytoplasmic roles, nuclear MYOVI is recruited to promoter and intragenic regions of active genes where it is able to co-localise with RNA polymerase II (RNAPII) in transcription factories. Downregulation of MYOVI has been seen to result in a decrease of steady-state mRNA(12). Its role in epithelial cell migration, alongside the high expression levels seen in ovarian cancer, mean that it is currently a target for cancer therapy. Understanding it's interactions within cells and how dysregulation of its downstream targets results in cancerous phenotypes will undoubtedly be deciphered in the next decade of research. *MYOVI* is a downstream target of the estrogen receptor (*ER*), where activation of *ER* results in the upregulation of *MYOVI* transcription which is seen in aggressive cancer types. P53 typically safeguards this interaction by interfering with the binding of ERα to gene promoters via a positive feedback loop. In ER+ cancers *P53* is often mutated, losing its capability to bind *ERα* promoters, resulting in up-regulated ERα signaling and high expression of *MYOVI* (13).

Knockdown of *MYOVI* reduces the level of ER driven gene expression indicating that MYOVI plays a role in activating its transcriptional activity. Upregulation of *MYOVI* is commonly seen in several cancers as it is found to promote cell growth (14).

1.3: Functionality of DAB2

The 96kDa protein DAB2 is a known binding partner of the large insert (LI) isoform of Myosin VI through the WWY motif located in the CBD. Notably DAB2 possesses phosphotyrosine binding regions which facilitate interactions with receptors and other proteins, a proline rich region which interacts with Ras pathways and a SYF motif within which a Myosin VI binding site is located (15). The interaction between MYOVI and DAB2 allows controlled targeting of MYOVI to lipid membranes by dimerisation. The resultant increase of helicity within the tertiary structure, enables MYOVI's function as an endocytic motor, transporting and clustering transmembrane receptors close to a clatherin-coated pit(16).

DAB2 has been identified as a tumour suppressor due to its regulatory capability in proliferation, apoptosis and autophagy. One mechanism of action involves binding growth factor receptor binding protein 2 (GRB2), preventing its ability to activate C-FOS and MAPK(17). In cancer *DAB2* expression is often lost or highly limited due to hypermethylation of its promoter region(18).

1.4: Functionality of *ESR1*

Estrogens are involved in a whole host of biological systems within cells due to their functionality as nuclear receptors; these steroid hormone nuclear receptors are comprised of two genes, *ESR1* and *ESR2*, which encode ERα and ERβ respectively (19). We will be focusing on the function and structure of ERα as it is part of the fusion and interacts with *MYOVI*.

The structure of ERα, as seen in Diagram 1, consists of 2 transcriptional activation domains, the N-terminal ligand independent AF-1 and C-terminal ligand-dependant AF-2, the ligand binding domain (LBD), DNA-binding and hinge domains which are located in the core of the protein(20). Ligand binding to ER results in the recruitment of co-regulatory proteins and the binding of complexes to estrogen responsive element (ERE) sites. ERE's act in regulating the transcription of genes involved in numerous cellular processes. The ER responsive genes include

TP53 which is involved in regulating apoptosis, tumorigenesis and tumour progression(21) and cyclin-D1 which is involved in cell cycle progression through G1 (22).

Activation of *ER* in ER positive breast cancer cells causes cytoskeletal remodeling via the function of moesin on actin. These rapid and dynamic alterations are triggered by ERα interactions with G protein Ga_{13} which results in recruitment of RHO-A and ROCK-2 as part of a cascade. Reorganisation of the cytoskeleton interferes with focal adhesion sites and hence results in cell migration and invasion of distant tissue sites. (23)
Estrogen also enhances the activation of Ezrin via phosphorylation, a protein that binds actin and is seen to be overexpressed in breast cancer patients with a poor prognosis. This results in the downstream activation of PI3K. (24)

ER signaling from the plasma membrane allows RAS and PI3K to be activated resulting in signal transduction into the nuclear membrane by JNK, ERK1/2, p38 and NFkB. These are all involved in regulating cellular functions such a growth and apoptosis. In breast cancers, altered activation of these proteins results in unmediated growth and hence the formation of a tumour. Mutations in the LBD of ERα result in acquired resistance to initially effective therapies. The mechanism of this resistance is thought to involved the action of kinases, allowing the need for estrogen for activation to be bypassed (25, 26).

Tumours exhibit altered expression of ER coregulatory proteins such as metastasis associated protein 1 (MTA1), a transcriptional repressor of ER, which is commonly seen to be deregulated in breast cancers and hypoxia (27). The *MTA* family is comprised of MTA1, MTA2 and MTA3, which are 80kDa, 70kDa and 65kDa respectively polypeptides containing a BAH (bromo-adjacent homology) domain, ELM (eukaryotic linear motif) domain and SANT (Swi3, Ada2, MCor and TFIIIB) domain. The BAH domain is indicated to be involved in protein-protein interactions whereas the SANT domain allows interaction with histones within the nucleus (28).

1.5: *ESR1-DAB2* gene fusion

As mentioned previously, mutations in *ESR1* are commonly found in MBC patients, such as TP53. However, rare mutations involving translocations of deletions in *ESR1* are also seen to

pop up during screening, including the *ESR1-DAB2* fusion gene (Fig.22). The composition of the fusion gene can is highlighted in supplementary Figure 1, using Uniprot.org to allow the homologous regions of both genes to be visualized. Mapping of the fusion revealed that the DNA binding domain and hinge region of *ESR1* are maintained but the LBD is altered and is replaced by the majority of the *DAB2* gene (29). Genomic instability is a hallmark of cancer and is a result of defects in the DNA damage repair signaling pathway followed by the bypassing of cell cycle check points (30). Homologous recombination to attempt to repair the DNA can result in translocation of another gene where this break point can occur within a gene as seen in this fusion (31).

There is currently not repertoire of work on this construct and therefore it is unclear how it functions and why it is present specifically in MBC patients resistant to endocrine therapy. Elucidating the resultant protein's activity and interactions could allow for new therapeutic targets to be identified.

1.6: Hypoxia

While studying individual proteins or mutants in disease states is informative, it is important to consider the tumour microenvironment to fully understand the signalling pathways in play resulting in the observed phenotype. Hypoxia occurs when the oxygen demand of highly proliferative cells is not met. This stimulates PI3K, MAPK and NFkB pathways which then allow the cells to survive this adverse condition by activating autophagy to decrease the rate of oxidative metabolism (32). It can be classified into two major types; chronic or diffusion-limited hypoxia and acute or perfusion-limited hypoxia (33). Chronic hypoxia induces disassembly of the replisome and results in permanent damage to cells whereas acute hypoxia allows for recovery of metabolistic functions (34). Hypoxia is associated with aggressive tumour phenotypes due to its ability to enhance spontaneous metastasis by manipulating expression of E-cadherin and VEGF (35). Double strand breaks are also observed in hypoxia and downregulation of DNA repair systems results in genetic instability through the build-up of replication errors (90).

Hypoxic conditions specifically cause the activation of hypoxia inducible factor 1 (*HIF-1*). It functions as a hetero-dimeric protein and is involved as a transcription factor for a large number of target genes via its helix-loop-helix motifs that allow DNA binding. HIF's are comprised of a

HIFβ subunit and an oxygen- regulated α subunit (HIF-1α, HIF-2α or HIF-3α) (36). Downstream effects of this activation include the promotion of angiogenesis in hypoxic areas via binding with vascular endothelial growth factor's (VEGF) regulatory region and regulation of oxygen homeostasis. This signaling is seen to be up-regulated in cancer cells and hence is a key current therapeutical target (37). Previous research has revealed that hypoxia increases cancer stem cell characteristics which are distinctive from non-hypoxic tumour cell expression. The PI3K/AKT pathway is a key factor in accessing this stem cell-like phenotype and this overlaps with the estrogen signaling pathway seen in MCF7 where NFkB and CREB are activated within the nucleus.

Tumour hypoxia is typically associated with a poor patient survival. Therefore, it is specifically interesting to observe hypoxia induced changes in the localization and gene expression of proteins. In tumours, the central cells at the middle of the mass typically are necrotic due to the lack of oxygen (before the induction of angiogenesis) and thus, utilizing this stressor can allow progress to be made towards understanding how these cells survive and can be targeted within a tumour. (38) Hypoxic culture conditions can be achieved in a closed system incubator where all oxygen is removed. This can simulate the tumour microenvironment, enabling the impact of hypoxia on protein and processes of interest to be studied.

1.7: Aims

This study aimed to investigate the effect of intrinsic and extrinsic stressors on *MYOVI* expression and localization in order to determine potential interacting pathways. This is specifically important in respect of the cancer field as *MYOVI* is up-regulated in aggressive tumours. Therefore its interactions and signaling pathways are of interest for drug targeting and for use as biomarkers, potentially allowing the best method of treatment to be determined for each patient.

As an intrinsic stressor, we utilized a fusion gene isolated from a therapy resistant breast cancer patient, the *ESR1-DAB2* fusion. Dysregulation and mutations in *ESR1* signaling are commonly seen in aggressive cancers and Dab2 has not only been characterized as a tumour suppressor, but it also acts as a binding partner to allow targeted binding of MYOVI LI to lipid membranes. Therefore, the introduction of *ESR1-DAB2* into HeLa and MCF7 was performed in order to

characterize its localization and suggest a potential function, especially with regard to MYOVI localization.

MCF7 is a human breast adenocarcinoma cell line initially derived in 1970 from malignant adenocarcinoma. Within the breast cancer field it is the most studied cell line due its stability in adherent culture, fast replicative prowess and genomic stability in comparison to other cancer cell lines which exhibit large variations in chromosome number. This cell line has preserved its functionality to process estradiol via estrogen receptor alpha (ERα) and is therefore extremely useful in monitoring hormone induced expression changes and resistance. They have lost expression of *DAB2* and hence are a good target for the study of the *ESR1-DAB2* fusion as any DAB2 epitope picked up through biochemical assays will only be provided by the DAB2 portion of the fusion and not endogenous expression. (39)

The HeLa cell line, originally derived from Henrietta Lacks' cervical cancer in 1951, is one of the most used cell lines in biomedical science. These cells exhibit high numbers of chromosomes due to replicative errors (instead of 46 chromosomes they often have 76-80 chromosomes) but are advantageous in cell work as they grow extremely fast. This high proliferative rate can be attributed to the 10-50 copies of HPV18 genome and the E6 and E7 oncoproteins from the human papillomavirus (HPV) (91). Replicative errors are due to the insertion of a *HPV* genome near the myc proto-oncogene in the genome resulting in rapid and endless replication as a result of the activated expression of telomerase (40). Unlike MCF7 HeLa have conserved the expression of *DAB2* but instead have lost the expression of *ER*. Using the differences between the two cell lines in this way allows the functionality of MYOVI to be compared in both hypoxic and transfected conditions.

The use of both cell lines allows for a comparative analysis of *ESR1-DAB2*'s functionality in both ER+ ad ER- cell lines and could shed some light on why this specific mutation favors MBC.

The extrinsic stressor, hypoxia, is seen in patients with higher levels of metastasis and also results in resistance to radiotherapy and chemotherapy in some patients. Study of its effects is invaluable to examine the endogenous expression of *MYOVI* and ERα/DAB2 in MCF7 and HeLa respectively, revealing more about the activated signaling pathways in this state.

2.0: Materials and methods:

2.1: Cell culture

HeLa (ECACC 9301013) and MCF7 (ECACC 86012803) cell lines were cultured in Gibco MEM media supplemented with 10% fetal bovine serum and a combination antibiotic composed of 100 units/ml penicillin and 100µg ml^{-1} streptomycin (MEM-complete). Sterile plates or flasks were incubated at 37°C with 5% CO_2. Adherent cells are washed with sterile and filtered PBS before being trypsinised with trypsin 0.05% EDTA. Following 5 further minutes of incubation cells detach from plastic surface and can be counted. Cells are typically grown to 70-80% confluency and were only used for experiments between passages 3 and 25.

2.2: Transfections

Transfections were performed in 24 well plates on both MCF7 and HeLa cell lines using Lipofectamine 2000 (Invitrogen) as the transfection reagent. 500ng of the ESR1-Dab2 plasmid was added to 1µl of lipofectamine in opti-MEM and applied to the cells in antibiotic deficient media. The media was then changed back to complete after 5 hours and the cells were fixed after 48 hours.

Electroporation was also employed in which $2.5x10^6$ cells were resuspended in Gibco opti-MEM media with 25µg/ml DNA in 0.2cm cuvettes. Exponential decay mode was selected where the voltage was set to 300, capacitance at 500uF and the decay curve registered between 4.5 and 4.8ms pulse time. The sample was then immediately seeded into a 6 well plate or 24 well plate with pre-warmed MEM-complete media.

2.3: Immunofluorescence (IF)

Growth medium was removed from transfected and hypoxic cells before washing with PBS. In the case of hypoxic cells all stages of fixation were performed within the sealed hood at 37°C to prevent a reversion to normal metabolic function upon exposure to oxygen. Transfected samples were fixed at room temperature. 4% (w/v) paraformaldehyde was applied to wells for 15 minutes followed by quenching using 50mM ammonium chloride for a further 15 minutes. The nuclear

DNA was stained via a 10 minute incubation using 1µg ml^{-1} Hoechst 33342 (Thermofisher) in PBS.

Post fixation cells were permeabilized and blocked with 3% (w/v) BSA in PBS, supplemented with 0.1%(w/v) Triton X-100, before being covered and incubated for 1.5 hours in the primary antibody at the appropriate dilution in 3% (w/v) BSA in PBS. The cover slips were then washed in 0.2%(w/v) BSA 0.05%(w/v) Triton X-100 in PBS three times and the secondary antibody was applied at the appropriate dilution in 3% (w/v) BSA in PBS, before covering and incubating for 1 hour. All steps post-fixation were performed at room temperature for transfected and hypoxic experiments.
All antibodies used for experiments are listed with their corresponding optimized dilutions.

Primary antibodies used:

- Abcam anti-Dab2 antibody (ab88590) mouse polyclonal 1:100 dilution
- Abcam anti-HA tag antibody (ab18181) mouse monoclonal 1:200 dilution
- Sigma anti-MYO6 antibody (HPA035483) rabbit polyclonal 1:200 dilution
- Anti-ERα antibody (sc-8002: santa cruz biotechnology) mouse monoclonal 1:100 dilution

Secondary antibodies:

- Anti- mouse Alexa 488 (green) antibody
- Anti- rabbit alexa 555 1:500 dilution

The cover slips were washed once again with PBS before mounting onto slides using Mowiol (10% (w/v) mowiol, 25% (w/v) glycerol, 0.2M Tris-HCL, pH8.5) supplemented with the antifading reagent DABCO (Sigma #D-2522).

2.4: RNA extraction and PCR

- RNA extraction:

  1ml of cold trizol was added to $1x10^6$ cells before incubation at room temperature for 5 minutes. 200µl of chloroform was added to the cell lysate and incubated for 2 further minutes at room temperature before centrifugation at 12000g for 15 minutes at 4°C.

The top aqueous phase (containing RNA) was transferred to a clean microcentrifuge tube and 500µ of isopropanol was added then incubated for 10 minutes. The sample was centrifuged at 12000g for 10 minutes at 4°C. The supernatant was disarded and pellet resuspended in 1ml of 75% ethanol then vortexed and centrifuged for 5 minutes at 7500g at 4°C. The supernatant was once again discarded and pellet washed with ethanol again before being left to air dry in a fume hood. Pellet was then resuspended in 20-30µl of RNAse-free water and incubated on a heat block at 60°C for 15 minutes.

The RNA concentration was then measured using a nanodrop. 500ng/ul final concentration was achieved by diluting RNA samples with water. 1ul was then carried forward into cDNA synthesis.

- cDNA synthesis:

cDNA synthesis was performed using abm's onescript cDNA synthesis kit and protocol.

- PCR:

PCR was performed using Pfu Phusion protocol supplied by new England biolabs. cDNA was diluted to a 1/10 mix and a 100mM stock of each primer was diluted to 10mM. The total reaction volume was adjusted to be 20µl. Samples were loaded into techne 3 prime personal thermal cycler where the cycling programme was as follows:

Denaturation: 98°C, 30 seconds
25-35 cycles: 98°C, 5 seconds
Annealing: 72°C 15-30 seconds/kb
Final extension: 72°C, 10 minutes
Hold: 5°C

- qPCR:

qPCR was performed on cDNA samples (1ng) obtained from onescript kit using green-2-go qPCFR mastermix supplied by biobasic. The expected band size of ESR1 is 51bp.

2.5: Hypoxic culture:

Cell lines were seeded into 24 well plates at a stock concentration of $2.3x10^5$ cells/ml. Incubation was undertaken for 5 and 24 hours where cells were fixed or scraped within the hypoxic hood. Conditions were set to 37°C, 0% O_2 substituted with N_2 and 5% CO_2.

2.6: Immunoblotting

MCF7 and HeLa cells were scraped off the culture dishes and centrifuged for 10 minutes at 500xg to form a pellet at 4°C. The cell pellets were then lysed using a lysis buffer comprised of stock reagents 4x NuPAGE SDS- sample buffer (thermofisher scientific), 1x PBS and 1 M DTT in a 4:4:2 ratio before being run on an 8% acrylamide gel, along with PageRuler Plus Prestained Protein Ladder. The gel was then immersed in running buffer with 1% methanol. The running buffer was diluted to 1x from a 10x tris-glycine SDS stock solution (25mM Tris base, 192mM glycine, 1% SDS at pH 8.3).

The PVDF membrane was activated by 100% methanol soaking for 1 minute before being rinse thoroughly and submerged in transfer buffer (NuPage transfer buffer by thermofisher scientific) on a rocker for 5 minutes. The fiber pads were also soaked in transfer buffer before being stacked in the transfer pad. Once the proteins have been transferred onto the PVDF membrane it was placed in blocking methanol (10%) for 5 minutes and washed before being soaked in blocking buffer (5% milk in TBS enriched with 0.1% tween) for a minimum of 1 hour. The primary antibody is then added to the blot in blocking buffer at the appropriate dilution and incubated on a rocker for 1.5 hours. The membrane was then washed with washing buffer (1% milk in TBS, enriched with 0.1% tween) three times at 10 minute intervals before the secondary antibody was applied in blocking buffer at the appropriate dilution and incubated on the rocker for 1 hour.

Primary antibodies:

- Sigma anti-MYO6 antibody (HPA035483) rabbit polyclonal 1:500 dilution
- Anti-ERα antibody (sc-8002: santa cruz biotechnology) mouse monoclonal 1:100 dilution
- Abcam anti-Dab2 antibody (ab88590) mouse polyclonal 1:1000 dilution
- Abcam anti-HA tag antibody (ab18181) mouse monoclonal 1:1000 dilution

Secondary antibodies:

- Abcam Goat Anti-mouse IgG (Hrp) (ab97023) 1:15000 dilution
- Abcam goat anti-rabbit IgG (Hrp) (ab6721) 1:15000 dilution

To image the secondary antibodies ECL western blotting detector reagents (Invitrogen) were used following the product protocol and blots were then imaged using Syngene Gbox which acquired images through Genesys software.

2.7: Imaging

Initial experimental cell imaging was performed using the Zeiss confocal microscope where mounted samples were illuminated with LSM 880 lazer light source using the appropriate filters. Zen Black was then used capture and save images images. The 100x lens was used to obtain images where a z-stack through the nucleus was used to obtain cell slices and the middle slice was used.

Further imaging was executed using the Olympus BX-61 epifluorescence microscope equipped with cooled CCD camera using SmartCapture 3 software (digital scientific, UK) to capture and save images.

2.8: Image analysis

All images were analyzed using imageJ. Image quantification was performed by calculating the corrected total cell fluorescence (CTCF);

$$CTCF = (integrated\ density - (area\ of\ selected\ cell \times mean\ fluorescence\ of\ background\ readings)$$

The mean fluorescence was calculated from the CTCF of three images, for both the red and green channels, where the minimum and maximum brightness and contrast was set to the same values.

Standard deviation of the samples was calculated in excel using the CTCF's obtained for each sample, followed by the standard error which was then displayed as error bars.

3.0: Results

3.1: Optimizing exogenous expression of *ESR1-DAB2* fusion in HeLa and MCF7 cells

Previous research into the functionality of the *ESR1-DAB2* fusion has exclusively been performed in HEK293 cells (human embryonic kidney cell line). Therefore, in order to acquire more informative results, it would be useful to investigate the behavior of this fusion protein in other cancer cell lines. MCF7, like HEK293, have lost the endogenous expression of *DAB2* but retain the expression of ESR1. HeLa however, express endogenous *DAB2*, but have lost expression of *ESR1*. For these reasons HeLa and MCF7 were chosen as representative models to observe the exogenous expression of the fusion protein.

The *ESR1-DAB2* plasmid is relatively large and therefore this can result in less efficient and effective transfection via normal practice. Consequently, this section mainly focuses on comparing lipid-based transfection and electroporation transfection to determine the most effective method for resultant expression of ESR1-Dab2 within HeLa and MCF7.

We hypothesized that the two proteins may interact as Dab2 is a binding partner of MYOVI. Therefore, double IF (dIF) was performed to observe the fusion and MYOVI simultaneously within samples, allowing any co-localization to be detected. In theory, due to the loss of endogenous ERα in HeLa, the control samples express no protein for the anti-ERα antibody to bind to and hence there will be no fluorescent signal. ESR1-DAB2 transfected HeLa cells should show a signal when probed for ERα, which we could identify as solely induced by the presence of the fusion protein. Similarly in MCF7, probing with an anti-DAB2 antibody would only elicit a signal from the resultant fusion protein, as this cell line has lost the endogenous expression of *DAB2*. The confocal images in figure 1 acted to test this theory and method of detection where electroporated MCF7 were probed with anti-DAB2 and anti-MYOVI primary antibodies while HeLa was probed with anti-ERα and anti-MYOVI primary antibodies

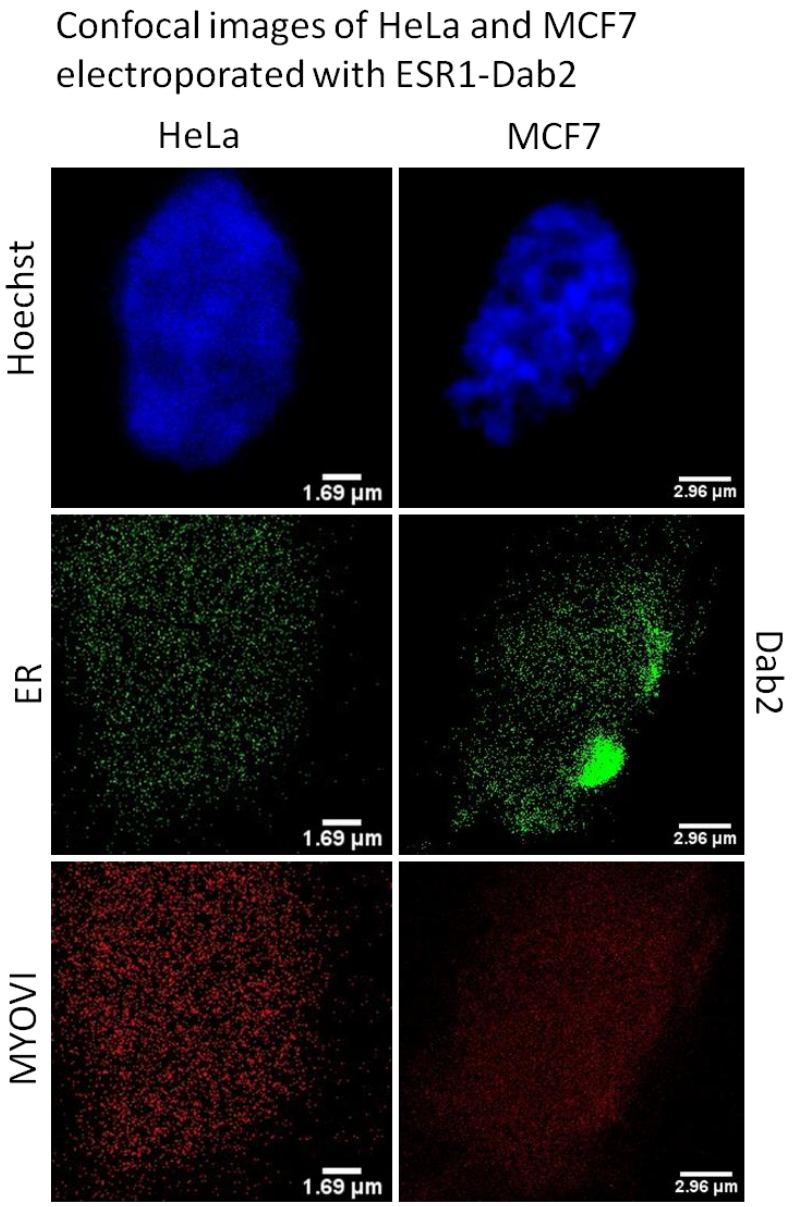

Figure 1: Confocal images of electroporated HeLa and MCF7 with ESR1-DAB2 where double IF was performed in order to image MYOVI and ESR1-Dab2 via anti-Erα in HeLa or anti-Dab2 in MCF7. Alexa647 and Alexa488 secondary antibodies were used respectively (HeLa Scale: 14.80 pixels/µm. MCF7 scale: 14.53 pixels/µm.)

In the process of these optimizations it should be mentioned that Figure 1 highlighted the lack of MYOVI fluorescence signal using the Alexa647 antibody. Due to the emission spectra of this fluorophore, we were limited to use of the confocal microscope, which still seemed to be unable to display a strong signal. As a result of this observation, future experiments employed Alexa555 as a secondary antibody to image MYOVI in transfections.

Examining protein levels within HeLa and MCF7

Microscopy is very useful in visualizing protein localization within cell lines, but is limited in terms of quantifying the amount of protein within the cell and nuclear compartment. Therefore,

western blots were performed to provide a more reliable indication of the levels of expressed MYOVI and ESR1-DAB2 within the cell lines which could then be supported by fluorescence intensity measurements obtained by microscopy.

Control Western Blots of non-transfected MCF7 and HeLa cells

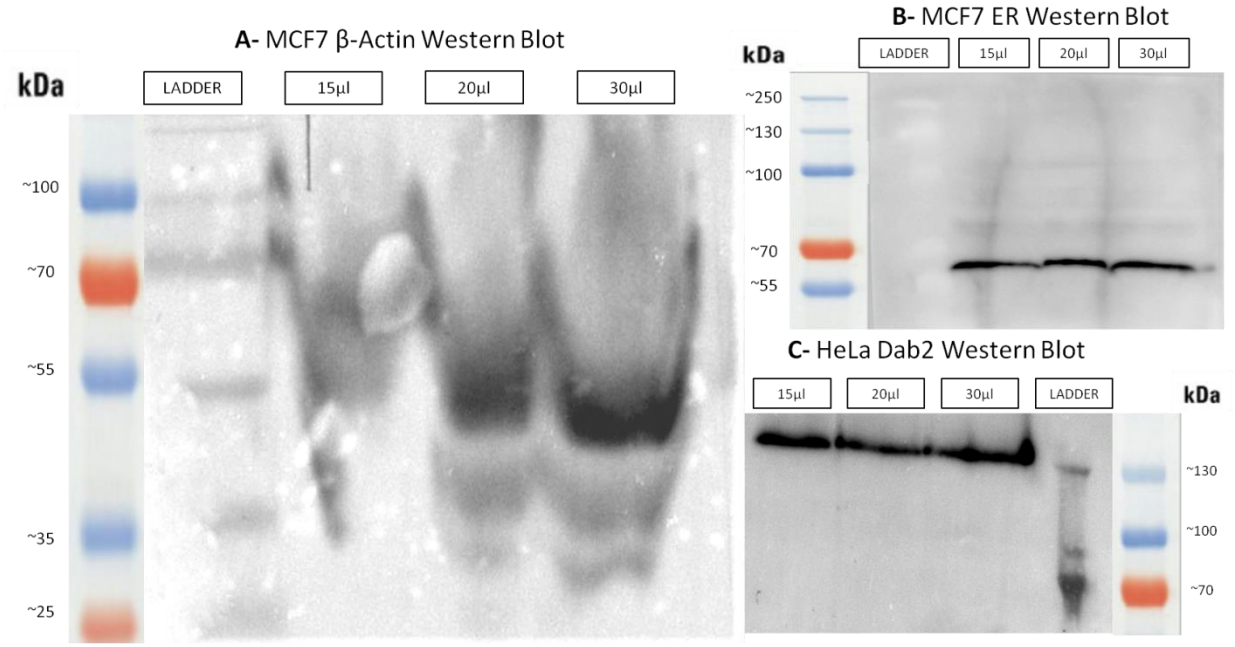

Figure 2: A – MCF7 cell lysate was run on a 8% gel before being transferred onto a western blot and probed for β-actin as a standard in order to confirm the western protocol was effective. B- MCF7 non-transfected cell lysate was run on an 8% gel and then probed for ERα in order to optimize the amount of antibody required in order to produce a clear band. C- HeLa non-transfected cell lysate was run on an 8% gel and probed to optimize the amount of antibody needed to display a defined band with minimal background/non-specific binding.

In order to characterize whether there was any change in MYOVI expression levels influenced by the introduction of *ESR1-DAB2*, western blotting was performed from lysed electroporated samples. Figure 2 shows the initial control blots using non-electroporated MCF7 and HeLa samples in order to ensure the method was optimized for use of ER and DAB2 antibodies and both cell lines. While the actin blot displays very dirty bands, we can obtain a distinct band using 20µl and 30µl of the sample and the band intensity shows a proportional increase when more sample is loaded. Figure 2B and C show that endogenous expression of ERα and DAB2, in

MCF7 and HeLa respectively, is easily detected in a western blot by probing with these two antibodies.

Positive controls were then performed on lysed electroporated MCF7 and HeLa samples, shown in Figure 3, to examine if the endogenous expression of these proteins was affected by the presence of the fusion and determine if endogenous expression was altered as a result of transfection stress. In the MCF7 left hand blot ERα appears as a band at ~65kDa and in the right hand HeLa blot DAB2 appears slightly below that expected at ~85kDa and seems to exhibit a weaker signal in ESR1-DAB2 transfected HeLa compared to the control. It was made clear from the HeLa blot that a higher volume (30µl) of the electroporated sample would need to be loaded in order to achieve a definitive band.

Control Western Blots of ESR1-Dab2 transfected MCF7 and HeLa cells

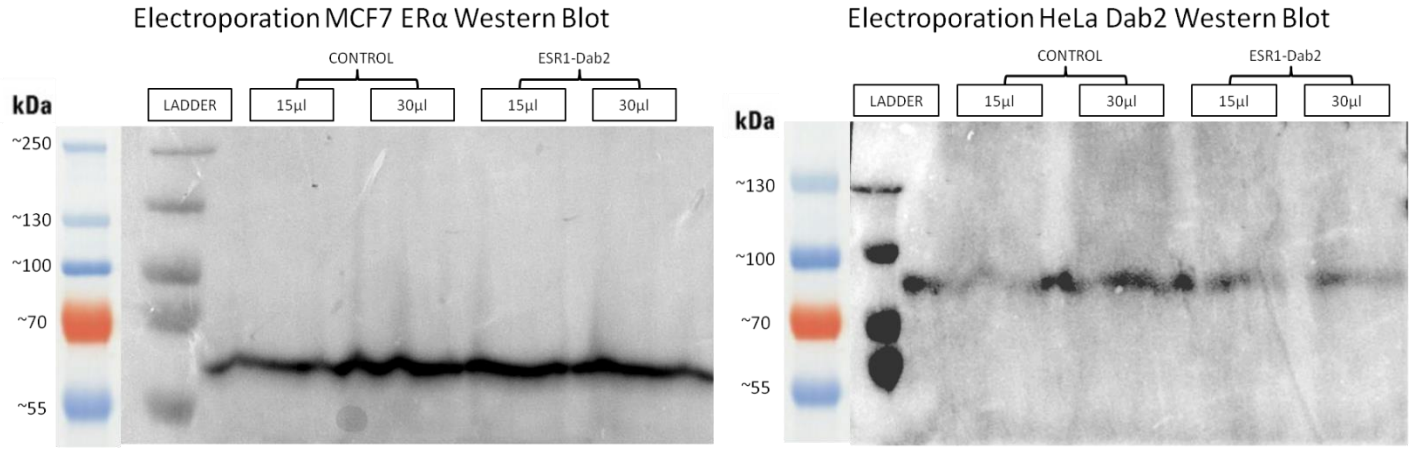

Figure 3: Electroporated cell lysates from MCF7 and HeLa were probed with ERα and Dab2 antibodies respectively as a positive control to determine optimum load to produce a clear band for endogenous protein and ensure sample viability for further western blotting.

Figure 4 shows the stripped western blot from Figure 3 which was then re-probed with MYOVI and ERα antibodies. Unfortunately this was unsuccessful in revealing a MYOVI band or an ERα band. Figure 5 followed the same procedure but was re-probed with DAB2 antibody instead of ERα. The western shows a band in both control and ESR1-DAB2 samples at ~150kDa, consistent with the presence of MYOVI, however it is not clear that the levels of MYOVI vary

between not only increasing the volume loaded but also between the control and the ESR1-DAB2 expressing samples.

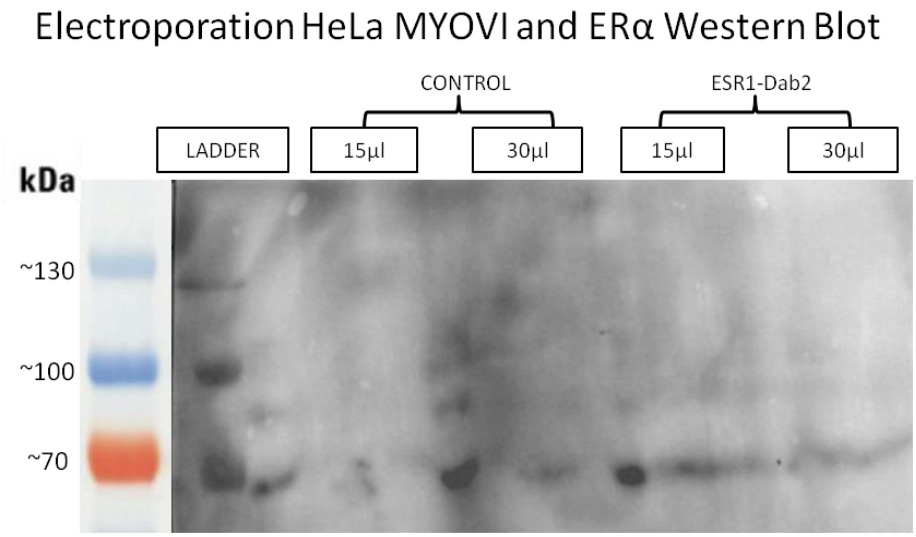

Figure 4: Reprobed western blot for Myosin VI and ERα (after stripping) of electroporated cell lysates from HeLa control and ESR1-DAB2 samples.

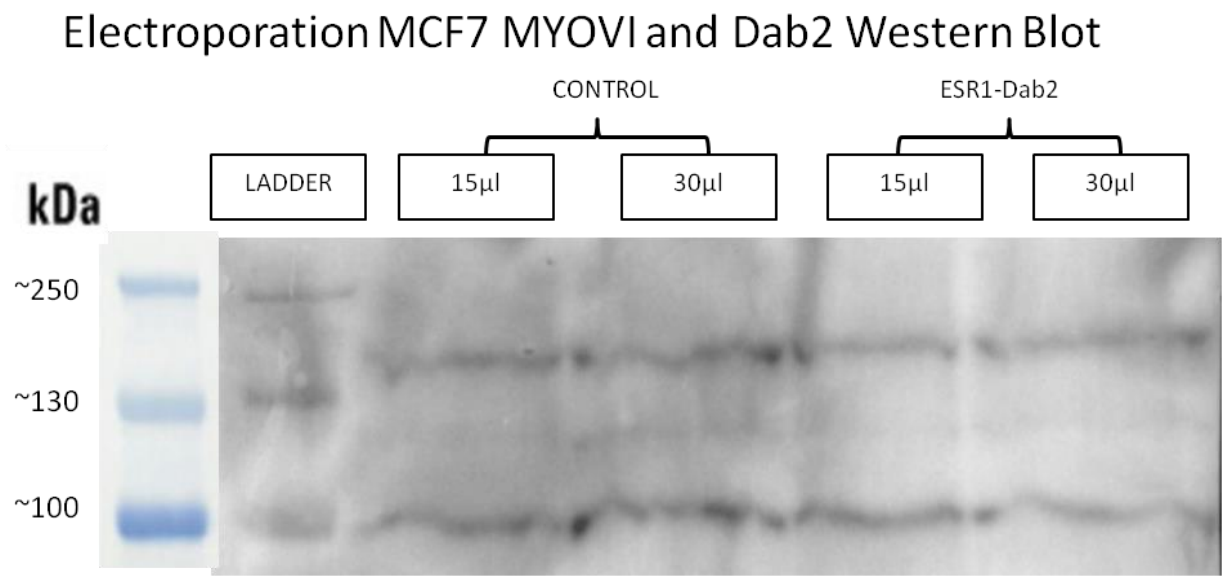

Figure 5: Reprobed western blot for myosin VI and DAB2 (after stripping) of electroporated cell lysates from MCF7 control and ESR1-DAB2 samples.

Unfortunately due to protein folding and the partial loss of epitopes within the fusion of the *ESR1* and *DAB2* genes result in ERα and DAB2 antibodies not effectively binding and therefore

in microscopy and western blotting the signal was not sufficient to confirm transfection. This was supported by the absence of the fusion in qPCR experiments shown in the supplementary material as the primers used (for ESR1 and DAB2 respectively) could not bind to the fusion. The preliminary transfections highlighted that these two antibodies were not viable to use in order to detect the fusion protein within samples. Hence, we had to determine another route to specifically detect the fusion, the most logical being to utilize the presence of the HA tag within the fusion. An anti-HA antibody was acquired and then used for all further dIF probing of samples, however westerns were unable to be performed due to our inability to acquire a HA positive sample in the time remaining. Microscopy using the HA antibody required additional optimization typically associated with utilizing a new antibody, ensuring that the previous dIF protocol was altered to elicit a clear signal. The following section displays the results of ESR1-Dab2 transfection via electroporation and lipofectamine methods where an anti-HA antibody is used to probe for ESR1-DAB2 expression in microscopy samples alongside MYOVI.

3.1A: Optimizing exogenous expression of *ESR1-DAB2* within HeLa

Microscopy of ESR1-DAB2 transfected HeLa cell line

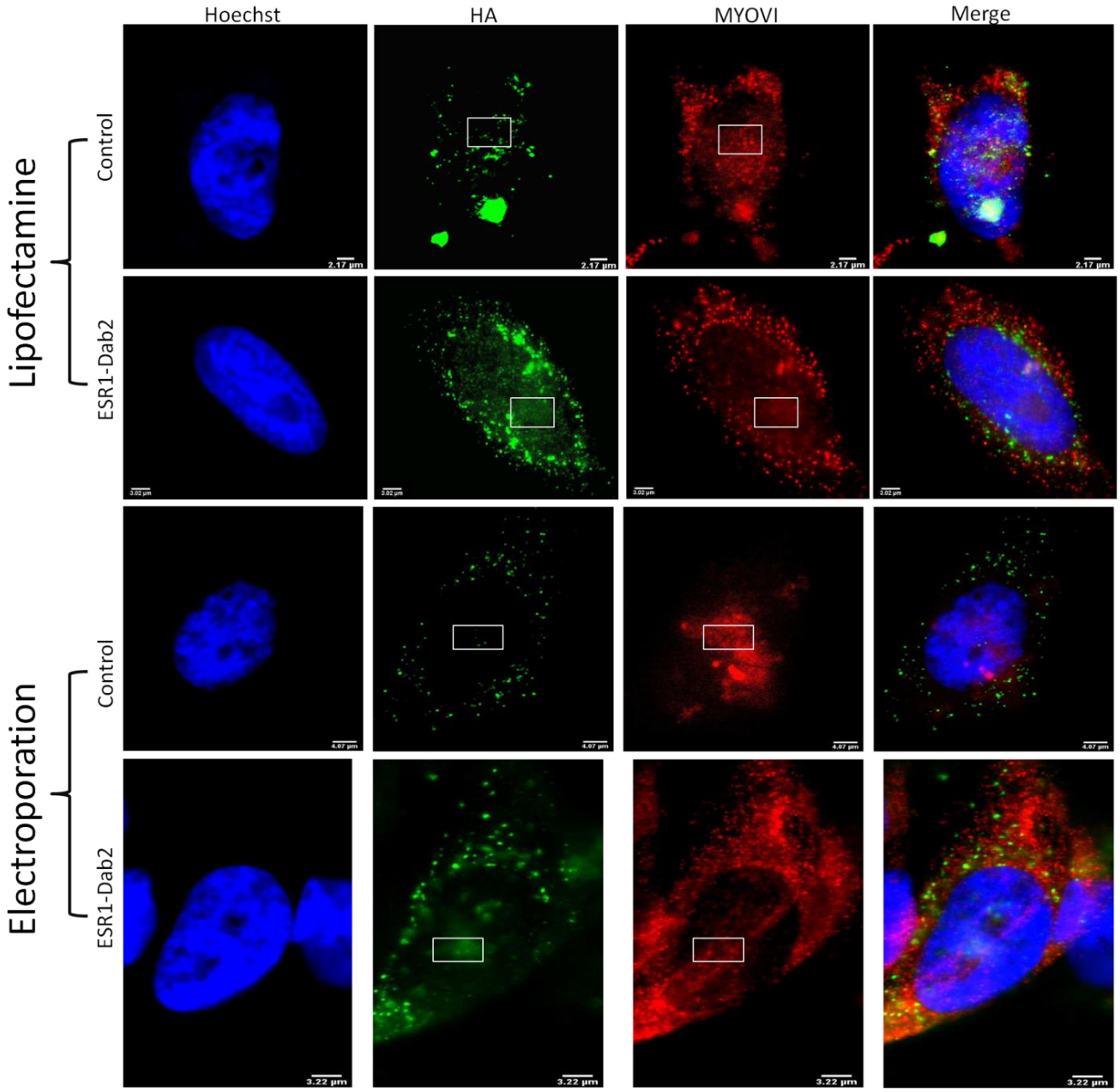

Figure 6: Images of HeLa cells transfected with ESR1-DAB2 plasmid using lipofectamine or electroporation. Immunofluorescence was performed post fixation using an anti-HA primary antibody alongside an anti-MYOVI antibody with alexa488 and 555 secondary antibodies respectively. Areas of interest are marked within the nucleus using imageJ to compare localization of both proteins in control and transfected states. (Scale: 15.215 pixels/µm)

Figure 6 shows transfection of the ESR1-DAB2 plasmid in HeLa using two common methods of transfection. In this cell line lipofectamine, a lipid based transfection method which induces the formation of liposome to ensure delivery of the plasmid, seems to result in more effective transfection as there is a visibly stronger HA signal. The HA antibody is infamously difficult to accurately image which is supported by the presence of a signal in both lipofectamine and electroporation controls. It is clear however that the HA signal is stronger in transfected cells and localized strongly to the periphery of the nuclear membrane as well as a small population of the protein displaying fluorescence inside the nucleus.

While the fluorescence intensity of MYOVI does not seem to vary between control and transfected samples, there is a definitive difference in the localization of the protein suggesting an effect of the presence of ESR1-DAB2 fusion on MYOVI distribution. MYOVI seems to localize strongly to the immediate periphery of the nucleus in both transfection conditions, with a reduction of the nuclear population seen in the transfected samples. Interestingly an unusual structure is visible in the electroporation sample which seems to span the center of the nucleus in a non-dividing cell and was observed in 33% of ESR1-DAB2 expressing cells.

Due to the nature of microscopy images it is difficult to use this data alone to arrive at a conclusion. Each individual cell may respond differently and fluorescence between cells can vary greatly. Therefore, in order to quantify this data and provide a more inclusive view of the effect of lipofectamine and electroporation transfections of ESR1-DAB2 the whole cell fluorescence intensity was measured from multiple cells within the sample to obtain a mean and this can be seen in figure 7.

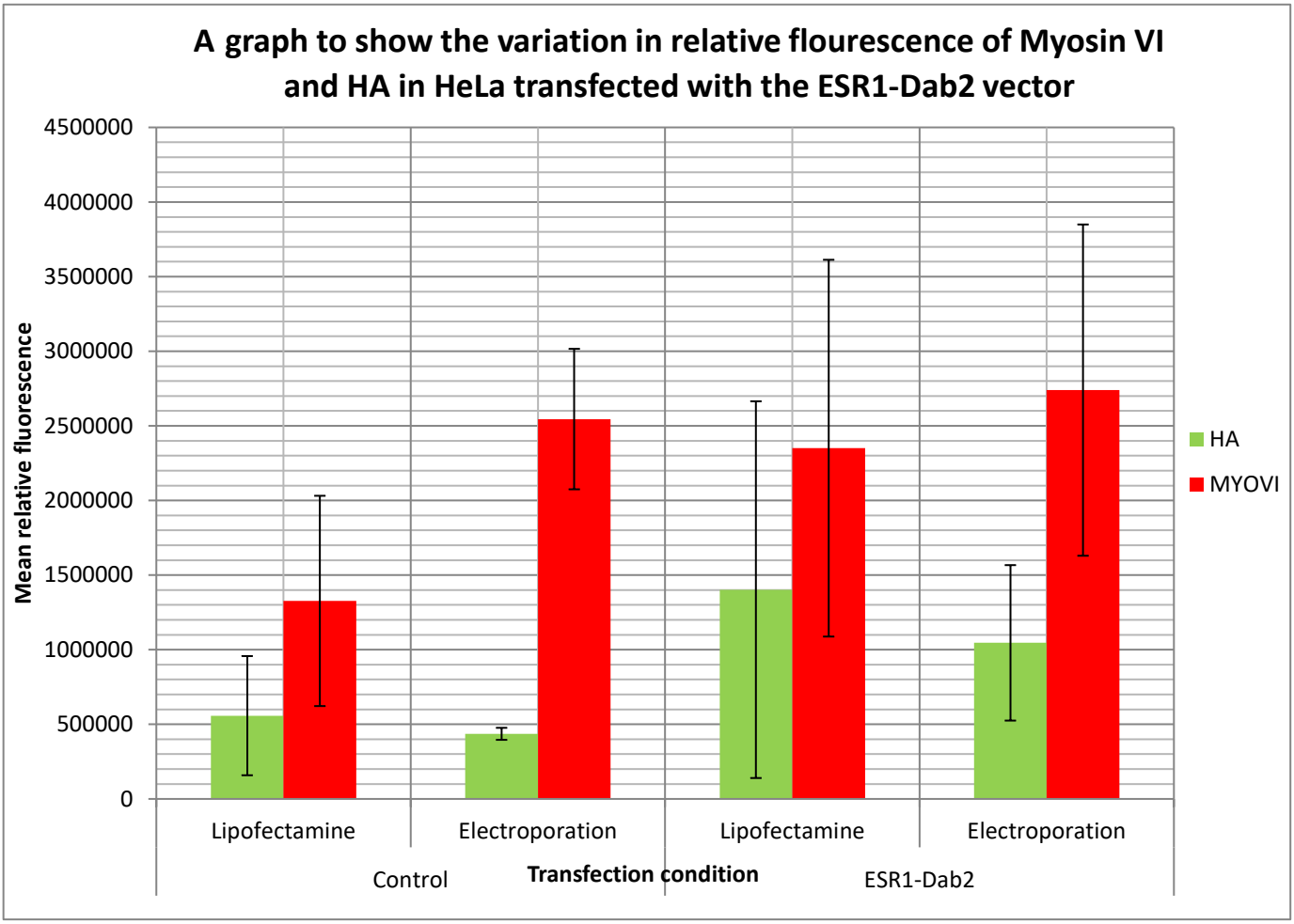

Figure 7: A Bar graph to show the quantification of mean fluorescence intensity in HeLa for both MYOVI and HA from each sample analyzed using imageJ. The standard deviation was also calculated to allow for calculation of standard error bars to be displayed. Three cells from separate cover slips were examined for each condition.

Figure 7 can be used alongside Figure 6 to infer the change in MYOVI and HA expression in HeLa between control and transfected samples. Reading from the bar graph, in HeLa there is little to no variation in the total cell MYOVI fluorescence between control and transfected samples in both methods of transfection. However, it is interesting to note that electroporation seems to cause a response that may be stress related seen in the elevation of MYOVI fluorescence in the control compared to the lipofectamine method. Using the images in Figure 6 we can say that while this fluorescence is as high as that observed in the transfected sample, the signal pattern of MYOVI changes within the nucleus in transfected samples, with an increase in

cytoplasmic signal suggesting altered function of MYOVI. HA fluorescence can be seen to increase slightly in transfected samples but the change in fluorescence seems minute when the error bars are taken into consideration. However, using the quantified data alongside the microscopy images infers that the cells are expressing the ESR1-DAB2 protein.

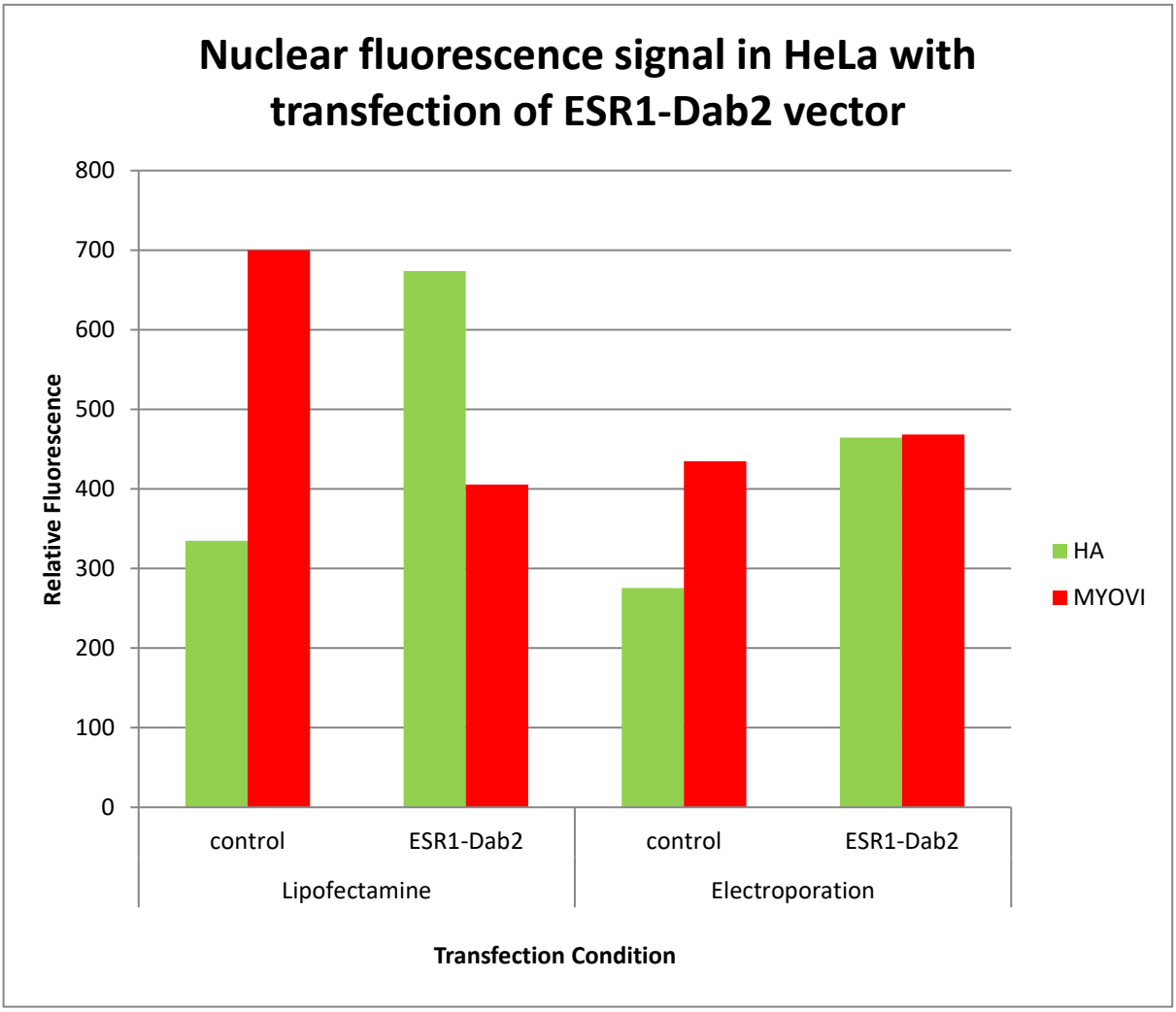

Figure 8: A Bar graph to show the quantification of fluorescence intensity in HeLa nuclei under transfection with lipofectamine and electroporation. The data corresponds directly to the marked nuclear zones seen in the microscopy images (Fig.6).

Figure 8 provides further insight into the change in localization of MYOVI and HA in both lipofectamine and electroporation transfections. It is clear that the method of transfection does affect the distribution of both proteins however in both there is an increase of HA within the

nucleus suggesting that the ESR1-DAB2 plasmid is present post transfection. Lipofectamine exhibits a more drastic increase in fluorescence between the control and the ESR1-DAB2 expressing cells within HeLa suggesting that this method is more effective than electroporation in allowing the plasmid to infiltrate this cell line. The levels of MYOVI seem to decrease in lipofectamine transfections; this suggests that while the total fluorescence increases (Fig.7), the population of MYOVI migrates to the nuclear periphery which is seen unanimously in ESR1-DAB2 expressing cells. In electroporation MYOVI fluorescence within the nucleus seems to be level and interestingly similar to the level of HA fluorescence in ESR1-Dab2 expressing cells. However HeLa seems to have poor transfection efficiency using this method and therefore this data is not conclusive.

3.1B: Optimizing exogenous expression of *ESR1-DAB2* in MCF7

Microscopy of ESR1-DAB2 transfected MCF7 cell line

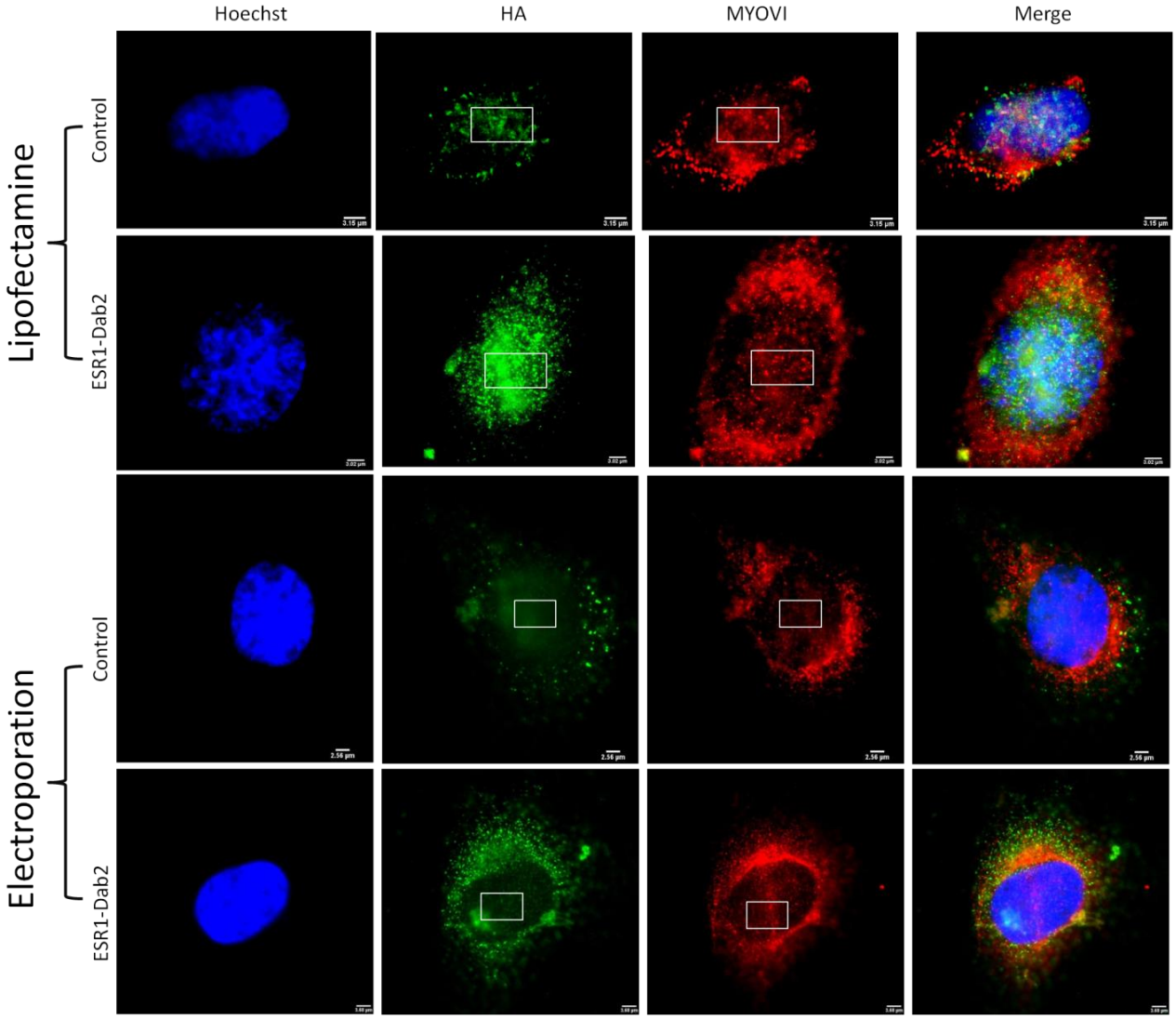

Figure 9: Images of transfection of ESR1-Dab2 plasmid in MCF7 using both lipofectamine and electroporation. Immunofluorescence was performed post fixation using an anti-HA primary antibody alongside an anti-MYOVI antibody with alexa488 and 555 secondary antibodies respectively. Areas of interest are marked within the nucleus using imageJ to compare localization of both proteins in control and transfected states. (Scale: 15.215 pixels/μm)

Figure 9 displays the images collected in the MCF7 breast cancer cell line after transfection with ESR1-DAB2 using lipofectamine and electroporation techniques. Visually there seems to be an

increase in the intensity of HA fluorescence suggesting that transfection was successful in this cell line using both transfection techniques. Examining first the lipofectamine transfected images, both the total and nuclear HA fluorescence increases when comparing the control and ESR1-DAB2 samples, with a large population of the ESR1-DAB2 protein seen to be residing within the nucleus. Transfection via electroporation also shows an increase in HA fluorescence, however the ESR1-DAB2 protein seems to collect on the nuclear periphery and not infiltrate the nucleus as vehemently as that seen by lipofectamine. Hence there seems to be a variation in localization and potentially then function of ESR1-DAB2 depending on the method of entry of the plasmid; using lipofectamine HA localizes strongly within the nucleus and the periphery whereas in electroporation the majority of the population of ESR1-DAB2 can be seen to localize at the nuclear periphery.

Once again as seen in Figure 6 in the HeLa cell line, total cell MYOVI fluorescence seems to remain constant, suggesting that expression of this motor protein is stable in MCF7 even after transfection stress. Figure 9 does reveal that localization is altered in both transfection methods between the control sample and the ESR1-DAB2 expressing cells. Lipofectamine transfection maintains a population of MYOVI within the nucleus seen in both the control and the ESR1-DAB2 expressing cells, however there seems to be a larger aggregation of MYOVI at the nuclear periphery visualized by the stronger fluorescent signal. In comparison electroporation seems to result in a smaller nuclear population of MYOVI in the control sample, so it is interesting to see the appearance of a similar structure to that observed in Figure 6 with HeLa electroporation in the ESR1-DAB2 expressing MCF7. Once again, the nucleus indicates that the cell is non-dividing and MYOVI also seems to collect at the periphery of the nuclear membrane with a less diffuse signal than the control.

From the merged images MYOVI also seems to co-localize with the ESR1-DAB2 fusion. This accounts for the different MYOVI localization patterns in lipofectamine and electroporated cells as the localization of the ESR1-DAB2 fusion determines the positioning of MYOVI within MCF7.

These images were further analyzed in order to quantify the results into numerical data, allowing a mean to be calculated from images of three separate cells under these conditions and this can be seen in Figure 10.

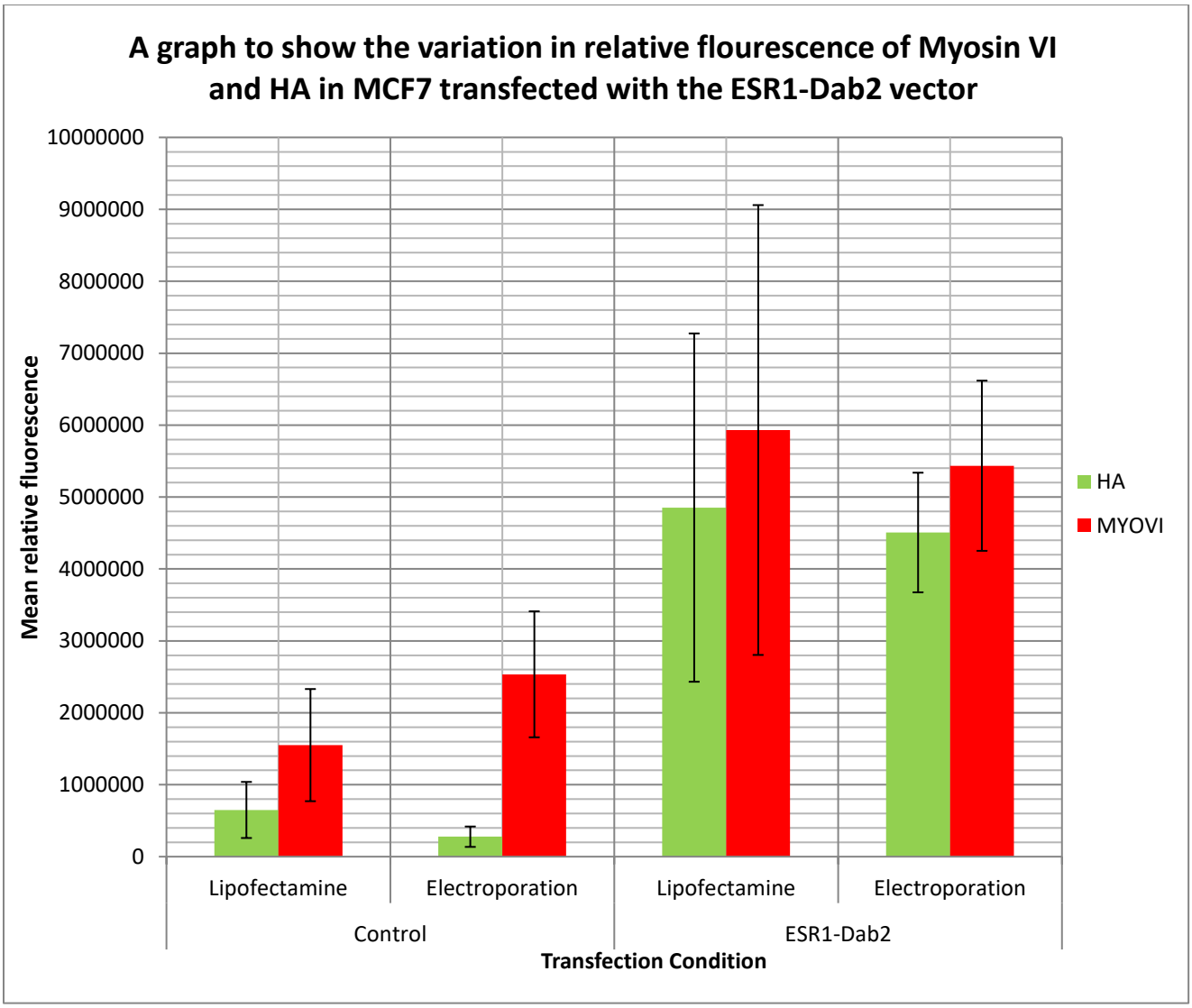

Figure 10: A Bar graph to show the quantification of mean fluorescence intensity in MCF7 for both MYOVI and HA from each sample 3 images of single cells from separate slides were analysed for each condition using imageJ. The standard deviation was also calculated to allow for standard error bars to be displayed.

From Figure 10 it is clear to see that the relative fluorescence fluctuates more in transfections using lipofectamine due to the size of the error bars. This suggests that in the case of MCF7, electroporation provides a more reliable set of data where both HA and MYOVI fluorescence in an individual cell is more closely representative of the whole population, where lipofectamine results in a large range of fluorescence and hence expression. Nevertheless, in both methods the mean total cell fluorescence of HA is seen to increase from the control to the ESR1-DAB2

expressing cells suggesting successful transfection and expression of ESR1-Dab2 within this cell line. Total cell MYOVI fluorescence is also seen to increase post transfection with lipofectamine and via electroporation. In both lipofectamine and electroporated ESR1-Dab2 expressing samples the total cell fluorescence of HA and MYOVI seem to be very similar therefore the localization of ESR1-Dab2 and MYOVI proteins was further quantified from Figure 9 to determine if they are concentrated within the nucleus or if their function lies within the cytoplasm.

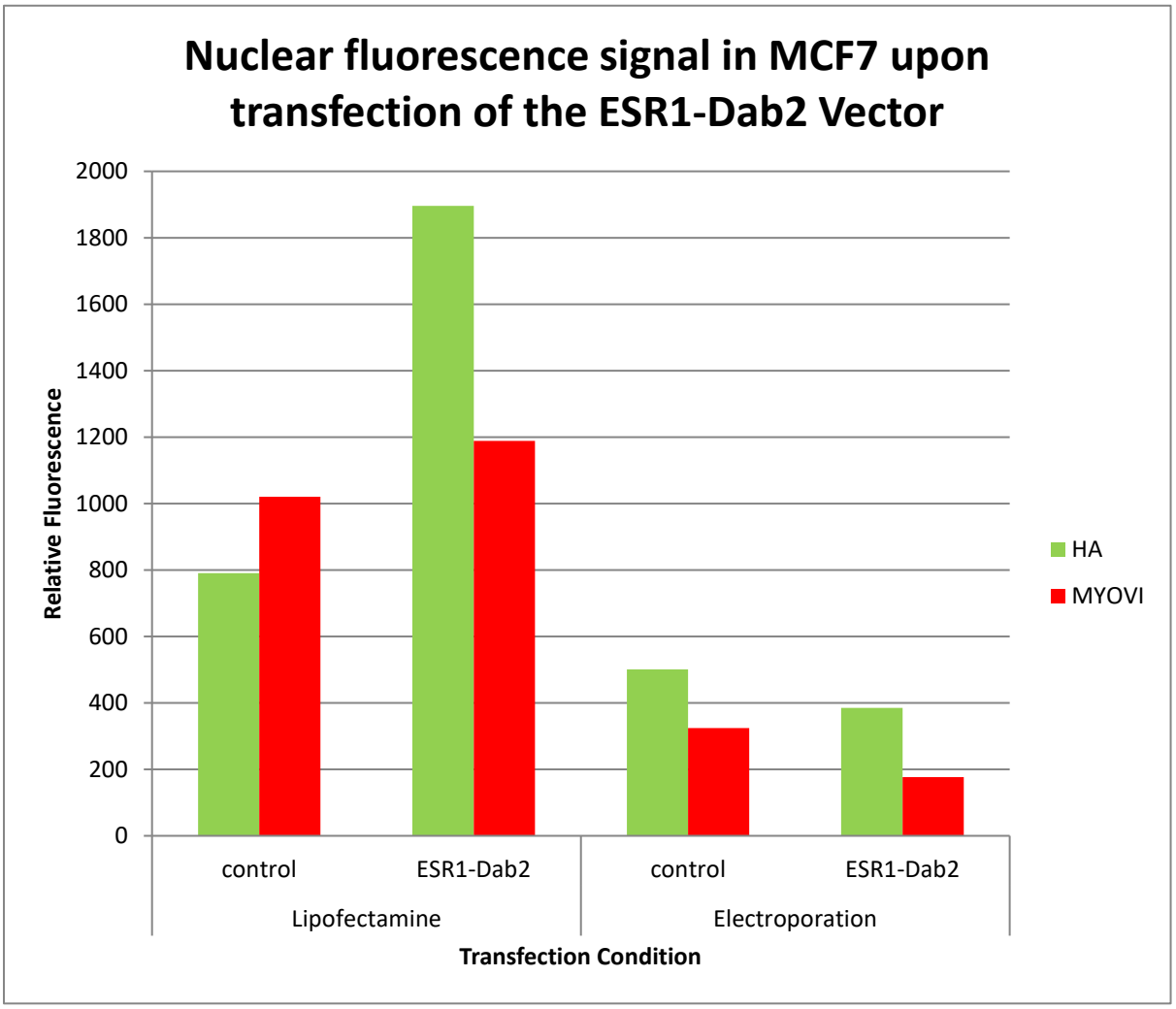

Figure 11: A Bar graph to show the quantification of fluorescence intensity in MCF7 nuclei post transfection with lipofectamine and electroporation in control and ESR1-Dab2 expressing samples. The data includes the marked nuclear zones seen in the microscopy images (Fig.9) and nuclear zones isolated from two other cells for each condition.

Comparing the data from Figure 10 and Figure 11 allows the localization of ESR1-DAB2 and MYOVI to be considered. During lipofectamine transfections, Figure 11 shows the population of ESR1-DAB2 within the nucleus increases drastically, visualized by the peak in HA fluorescence, whereas the levels of MYOVI seem to remain stable despite the increase in fluorescence seen in Fig.10. This suggests that MYOVI remains on the nuclear periphery and is correlates with the pattern of fluorescence observed in the microscopy images (Fig.9). From Figure 11, transfection by electroporation results in a negligible decrease in HA fluorescence within the nucleus of ESR1-DAB2 expressing cells. This is paired with a small decrease in MYOVI within the nucleus revealing that in addition to both proteins exhibiting similar fluorescence levels (Fig.10) they both seem to be confined to functions at the nuclear periphery and cytoplasm of MCF7 cells as observed in microscopy (Fig.9).

3.1C: Comparisson between MCF7 and HeLa

As HeLa and MCF7 cell lines were selected based on their varying endogenous expression profiles, it is integral to compare the effect of *ESR1-DAB2* transfection between the two to consolidate the differences in lipofectamine and electroporation transfection of this plasmid, providing some insight into the functionality of ESR1-DAB2 and the resultant localization of MYOVI in response to this intrinsic stressor. Figure 12 shows the data collected in sections 3.1A and 31.B side by side for ease of interpretation and comparison of quantified fluorescence between the two cell lines.

Figure 12A shows the mean relative total cell fluorescence of HA and MYOVI in transfections exclusively involving lipofectamine. In the control samples MCF7 and HeLa have similar levels of MYOVI fluorescence . HA fluorescence is higher in the MCF7 control sample than that in HeLa; however, in the ESR1-Dab2 samples this level seems to double in both cases. HeLa ESR1-Dab2 HA mean relative fluorescence seems to mirror the control levels in MCF7. Transfection using lipofectamine results in a dramatic increase in MYOVI levels within ESR1-DAB2 expressing MCF7, over double the value seen in ESR1-DAB2 expressing HeLa. Figure 12B shows the mean relative total cell fluorescence of HA and MYOVI following transfections by electroporation. Similarly to 12A MCF7 exhibit a much higher background HA signal in the control sample than HeLa, however the same pattern is observed as HA mean fluorescence doubles from the control to ESR1-Dab2 expressing cells. Interestingly the level of MYOVI fluorescence is very similar in both MCF7 and HeLa control samples, as well as the HeLa ESR1-DAB2 sample, and in tune with the lipofectamine results (Fig.12A) MYOVI is seen to have increased fluorescence in MCF7 expressing ESR1-DAB2.

Figure 12C allows all the data collected to be compared and from this we can see that the peaks of MYOVI fluorescence observed previously in MCF7 expressing ESR1-DAB2 (Fig.12A and Fig.12B) are at a very similar level in both lipofectamine and electroporation transfections. The same pattern can be observed between electroporated and lipofectamine transfected HeLa, suggesting that although localization seems to vary (Fig.6 and Fig.9), the effect of ESR1-DAB2 expression, regardless of the method of transfection, causes a standardized increase of MYOVI fluorescence in both cell lines.

Comparative analysis of HA and MYOVI relative fluorescence in transfected MCF7 and HeLa

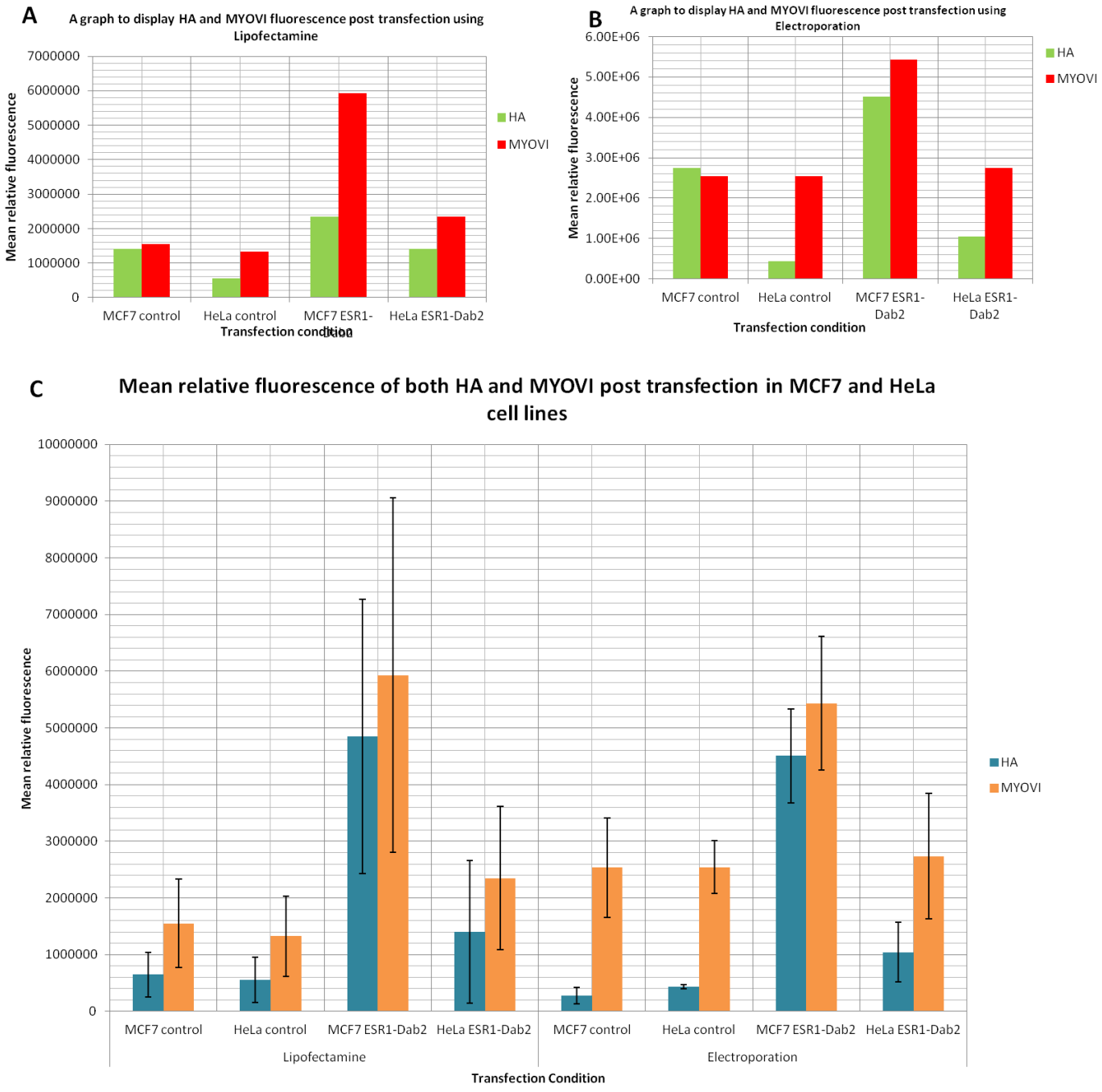

Figure 12: A- Mean relative fluorescence under lipofectamine transfections in both MCF7 and HeLa cell lines. B- Mean relative fluorescence under electroporation transfections in both MCF7 and HeLa cell lines. C- A cumulative graph of all the quantified data from imaged experiments described and imaged under section 3.1 involving transfection with ESR1-Dab2. All data was acquired using imageJ and the mean was calculated from 3 images for each condition. Error bars were calculated from raw data collected using standard deviation to calculate standard error.

Overall figure 12C shows that electroporation is a more reliable method of transfection for this large plasmid as the standard deviation covers a smaller range on either side of the mean fluorescence, indicating that the population of ESR1-DAB2 cells share a phenotype whereas lipofectamine transfections result in a broad range of fluorescence within the population of transfected cells. Despite this, electroporation in HeLa is not as effective as in MCF7 as shown by the incremental increase in HA and MYOVI fluorescence. In general the MCF7 cell line responds positively to transfection with ESR1-DAB2 whereas the data from HeLa seems to overlap between the control and transfected, hence is inconclusive and gives a limited insight into the function and interaction of ESR1-DAB2 within these cells.

3.2:Endogenous protein distribution in HeLa and MCF7 exposed to hypoxia

Exposing cells to hypoxia allows a more realistic view of protein expression and localization within a tumour mass microenvironment, before angiogenesis is activated to supply the cells with oxygen. This section therefore focuses on the localization of MYOVI and its binding/interacting proteins DAB2 and ERα within HeLa and MCF7 respectively over varying time periods of exposure to hypoxia. This may provide some insight into how these two cell lines survive in hypoxic states.

3.2A: Distribution of MYOVI and DAB2 in HeLa exposed to hypoxia

Microscopy of HeLa cell line exposed to hypoxia

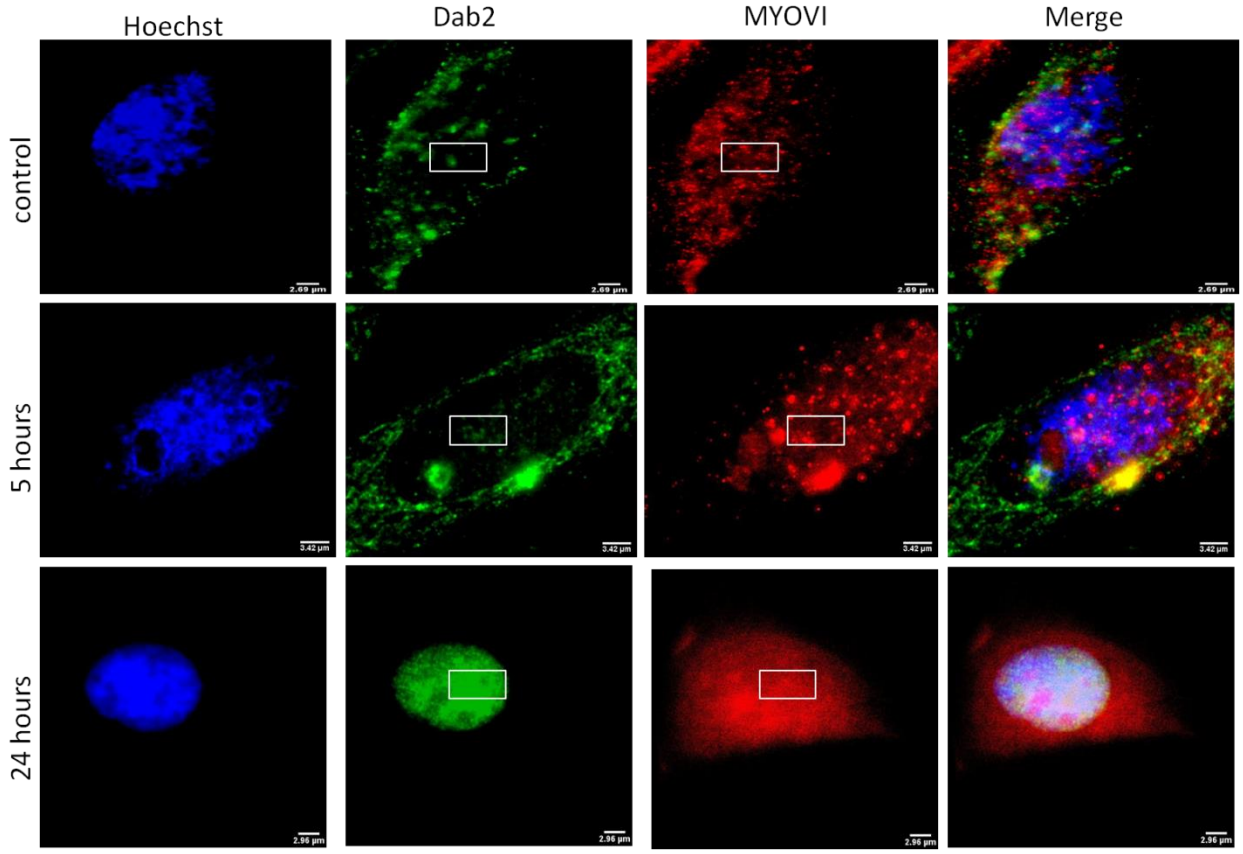

Figure 13: Microscopy of HeLa cells under 0, 5 and 24 hours hypoxia where immunofluorescence was used to visualize DAB2 and MYOVI localization and intensity with alexa488 and 555 respectively. Areas of interest within the nucleus are marked for further quantification and focused analysis.

The microscopy images seen in Figure 13 display the localization of endogenous MYOVI and DAB2 under varying time frames of hypoxic stress in HeLa cells. At a glance there seems to be very little difference between the control and the 5 hour 0% oxygen, 5% CO_2 condition, but the 24 hour sample shows dramatic change to the cells morphology and phenotype. Examination under the microscope displayed mass cell death in HeLa after 24 hours of hypoxic stress and the cells became filamentous in nature. This is visualized above as the nucleus is rounded where typically it would appear oval in shape such as that seen in the control and 5 hour samples. Dab2 can be seen to infiltrate the nucleus, displaying minimal cytoplasmic localization and this seems to be paired with MYOVI nuclear migration.

These images are limited in inferring the true change in localization and expression, therefore each sample was analyzed to collect quantitative data which is more representative of the population of cells in this condition, as opposed to a single image of a single cell.

Figure 14A displays the mean total cell fluorescence of MYOVI and Dab2 in HeLa during hypoxia. While the standard deviation overlaps for all samples, the quantification of data from several microscopy images allows a more representative result and conclusion to be formed. It is interesting to see that both Dab2 and MYOVI fluorescence levels peak at 5 hours in HeLa, before descending again at 24 hours to levels similar to that seen in the control samples. MYOVI total fluorescence doubles in this state in comparison to the control which was not previously evident in figure 13.

Figure 14B focuses on only the nuclear fluorescence of Dab2 and MYOVI within HeLa and shows a steady increase in MYOVI fluorescence intensity as the cells are exposed to hypoxia for longer. Furthermore, Dab2 nuclear fluorescence seems to double at 5 hours under hypoxia but still remains at a relatively low level in comparison to the massive peak seen in the 24 hour hypoxia sample. Using the data from figure 14B alongside the 24 hour microscopy image in Figure 13, the cell is not healthy and hence the spike in nuclear proteins could be attributed to the death of cells. Therefore, the most relevant data to examine in HeLa is the 5 hour hypoxia sample which shows increased mean Dab2 and MYOVI total fluorescence compared to the means observed in the control sample.

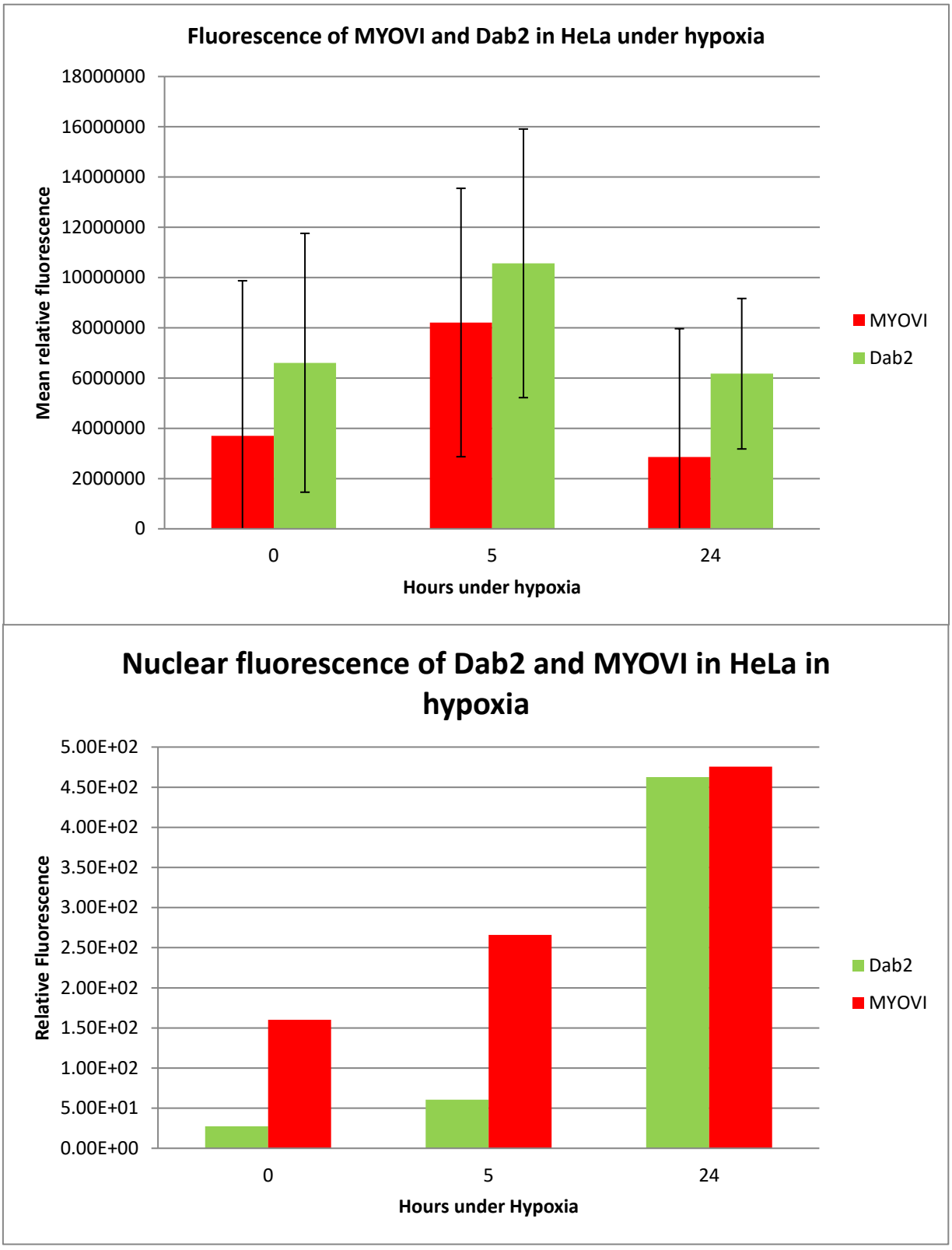

Figure 14: A- Quantified data from microscopy images acquired where the mean and standard deviation of fluorescence of MYOVI and DAB2 were calculated from 3 single cell microscopy images for each condition in HeLa. B- Quantified data from zones marked in microscopy images (Fig.13) and two further nuclei for each condition, displaying the nuclear fluorescence distribution of DAB2 and MYOVI with increasing time in hypoxic conditions

Figure 15 displays a western blot of cell lysate from each condition probed for MYOVI and DAB2. There seem to be bands present in the control sample and with 30µl of the 5 hour hypoxia cell lysate at ~100kDa indicating that this is the Dab2 band, however it is not clear that there is a difference in the amount of DAB2 present in these loads. Additionally, MYOVI does not present a band for any of these samples; therefore, further optimization is required to obtain a definitive result. Furthermore, the loading amounts need to be optimized to account for hypoxia induced cell death.

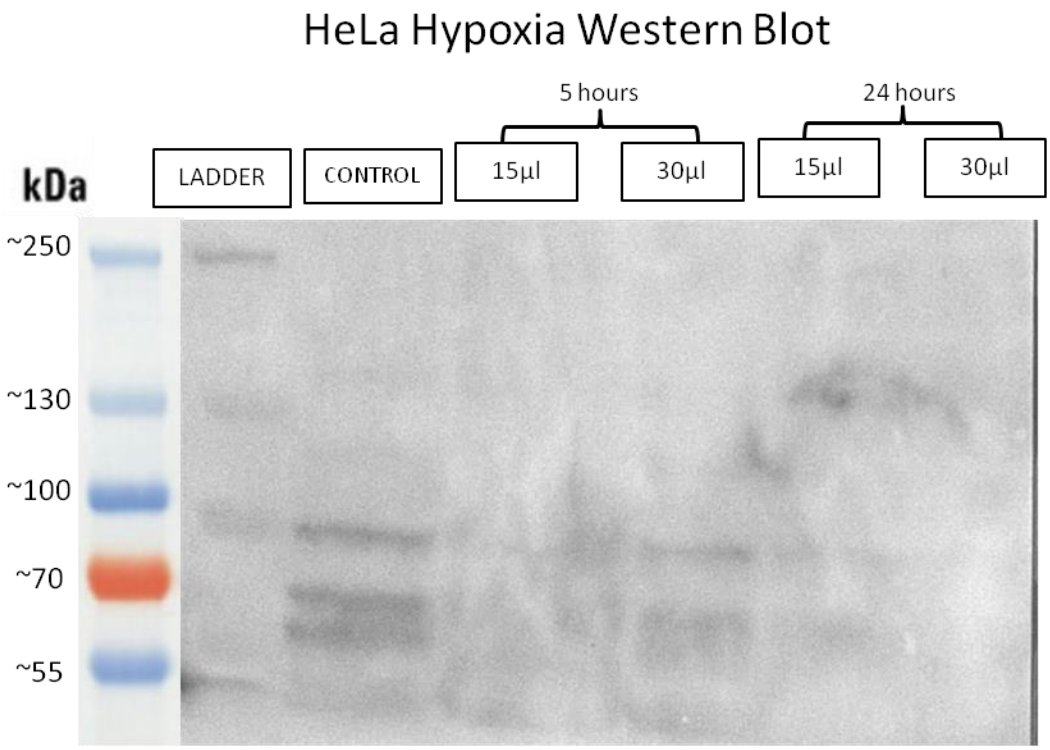

Figure 15: Western Blot analysis of HeLa cell lysate from cells exposed to hypoxia for 0 (control), 5 and 24 hours. 30µl of control sample was loaded and two volumes of each of the hypoxic samples. The western was probed with MYOVI and DAB2 antibodies.

3.2B: Distribution of MYOVI and ERα in MCF7 exposed to Hypoxia

The MCF7 cell line seemed to be more robust even after up to 24 hours exposure to hypoxia with minimal cell death and sustained 70-90% confluency. The phenotype did change mildly as cells became more adhesive and clumped together in masses, a typical reaction seen in MCF7 under stress, but as shown in Figure 16 the nucleus remained rounded in all experiments and the cellular membranes remained intact.

The control images show that ER is confined very strongly to the nucleus with no fluorescence displayed in the surrounding cytoplasm. MYOVI fluorescence however is diffuse throughout the cell. After 5 hours under hypoxia the ER fluorescence remains localized strictly to the nucleus while MYOVI seems to alter from the control with a population of this protein migrating into the nucleus and concentrating on the internal and external nuclear membrane.

Microscopy of MCF7 cell line exposed to hypoxia

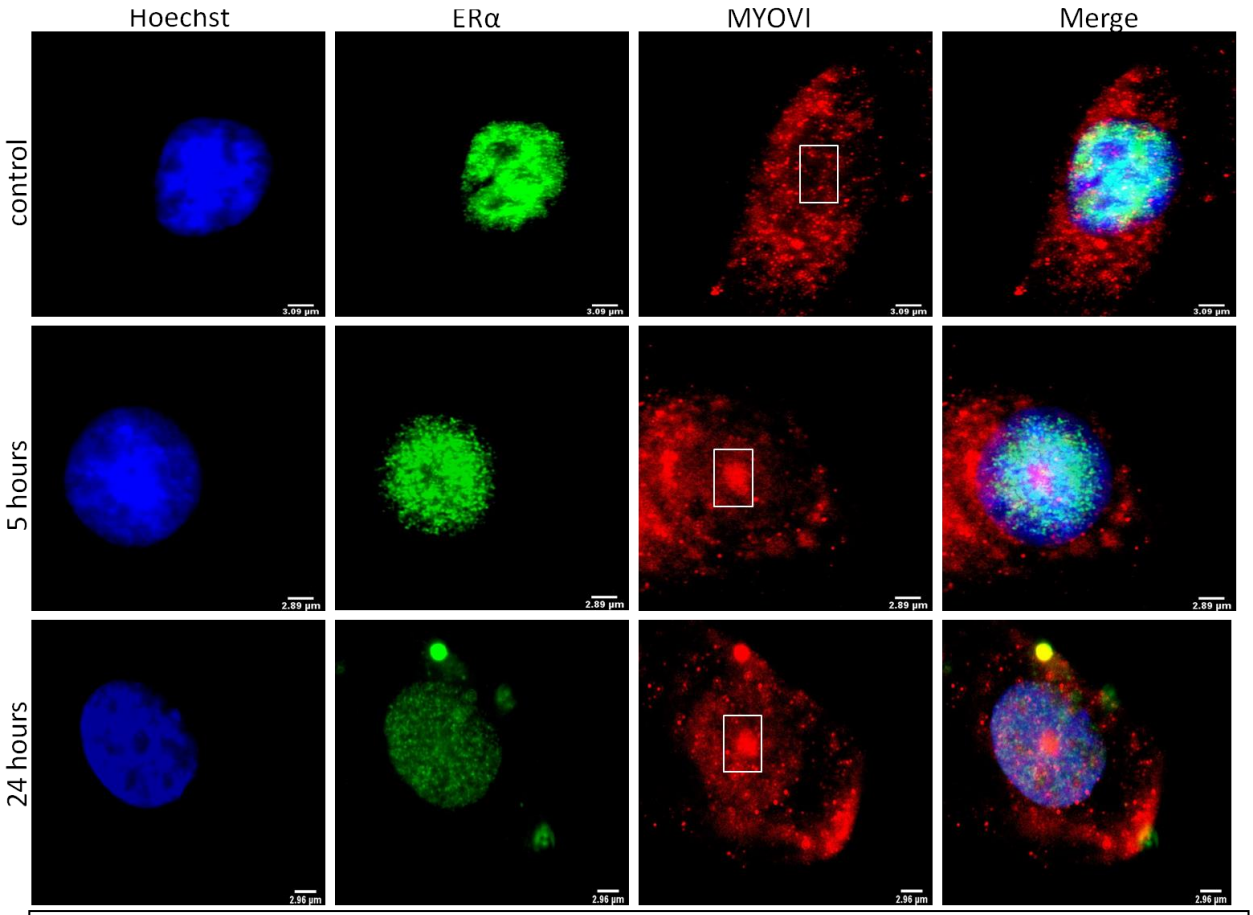

Figure 16: Microscopy of MCF7 cells under 0, 5 and 24 hours hypoxia where immunofluorescence was used to visualize ER and MYOVI localization and intensity with alexa488 and 555 respectively.

Interestingly there seems to be a clump of high fluorescence from MYOVI within the nucleus that is observed in both the 5 hour and 24 hour hypoxia samples. The 24 hour hypoxia images show reduced fluorescence from ERα while it is still confined to mainly the nucleus. MYOVI now shows an increased nuclear population as well as high fluorescence at apical membranes of the cell. The merged images for the 5 hour and 24 hour hypoxia samples show co-localization of nuclear MYOVI and ERα.

Figure 17 shows the nuclear fluorescence of MYOVI in these samples and indicates that there is an increase in the population of nuclear MYOVI as the hypoxia is maintained for longer amounts of time in MCF7.

Quantified data from a collection of microscopy images of MCF7 under hypoxia is displayed in Figure 18. While the nuclear fluorescence is seen to increase in MCF7 with increasing duration of hypoxia the mean total fluorescence of MYOVI observed within this cell line seems to be steady. It should be noted that the standard deviation is the largest at 5 hours suggesting that the MYOVI fluorescence at this stage exhibits a large range between cell samples measured and hence this level of stress may affect cells in different ways.

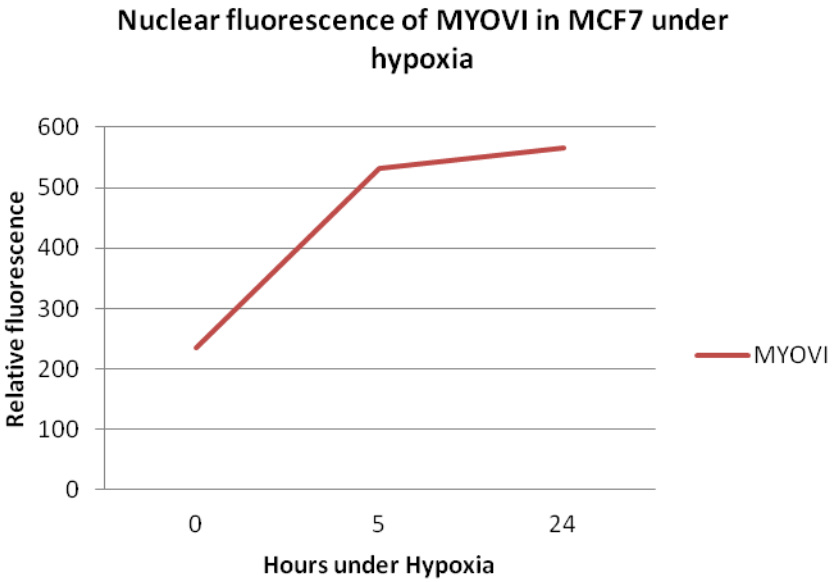

Figure 17: Quantified data from microscopy images specifically focused on MYOVI fluorescence within the nucleus during hypoxia. Fluorescence of 3 nuclei for each condition was averaged.

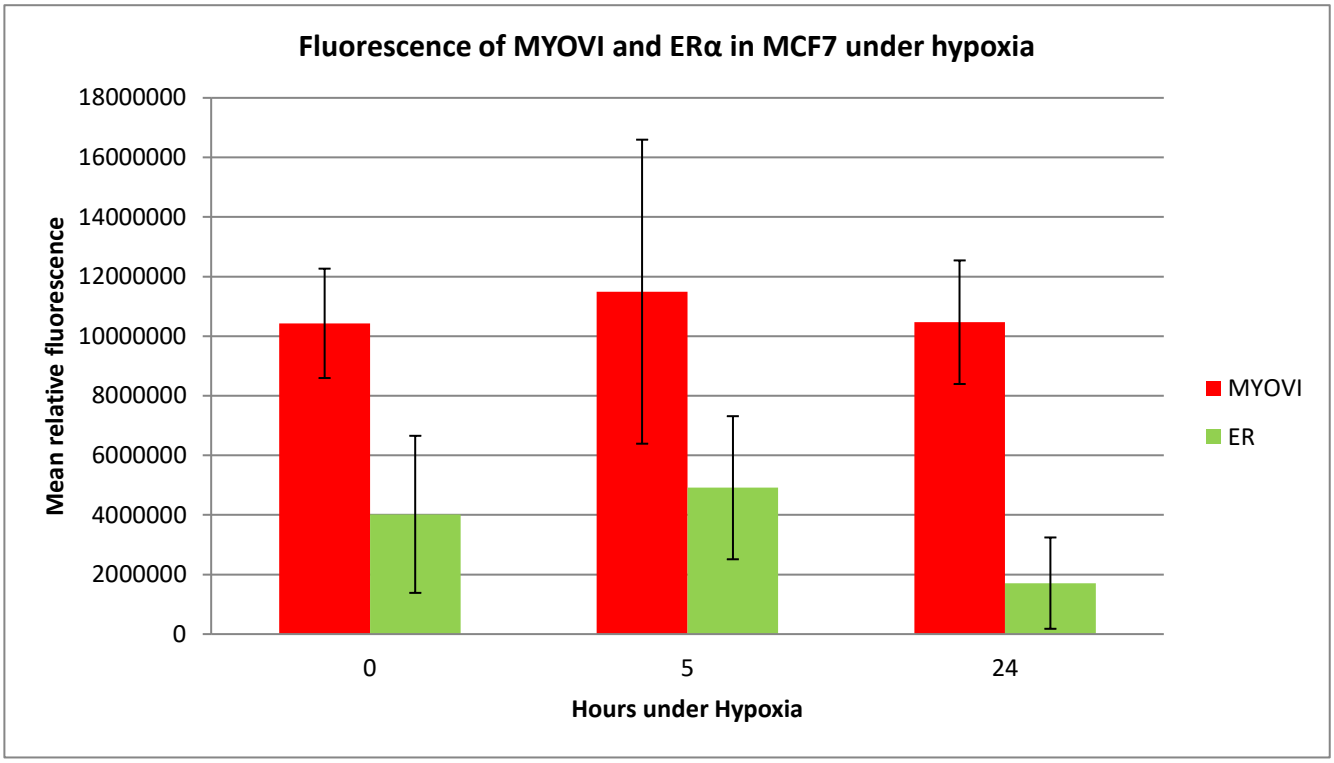

Figure 18: Quantified data from microscopic images displaying the mean total cell fluorescence of MYOVI and ER in MCF7 over varying time spans under hypoxia. Standard deviation was also calculated from the raw data collected before calculating standard error from several images of each condition. Three cells from separate slides for each condition were quantified.

Furthermore, the mean level of fluorescence of ERα within MCF7 remains relatively stable until exposed to 24 hour hypoxia where it is seen to decrease. As the signal is confined to the nucleus (Fig16) there was no need to measure the change in nuclear fluorescence to compare between samples as localization of ERα seems to be unaffected by hypoxia.

In a further attempt to quantify the amount of MYOVI and ERα expressed during hypoxia a western blot was performed as show in Figure 19. The MYOVI band appear at ~150kDa and is seen strongly in the control and 24 hour samples. When comparing the 0 hour 15µl load to the 24 hour 15µl load it seems that the intensity of the band has doubled. Unfortunately there is no band visible in the 5 hour samples, however the dark band at ~100kDa does resemble that of the other MYOVI bands but may be due to a load or sample preparation error and would need to be repeated.

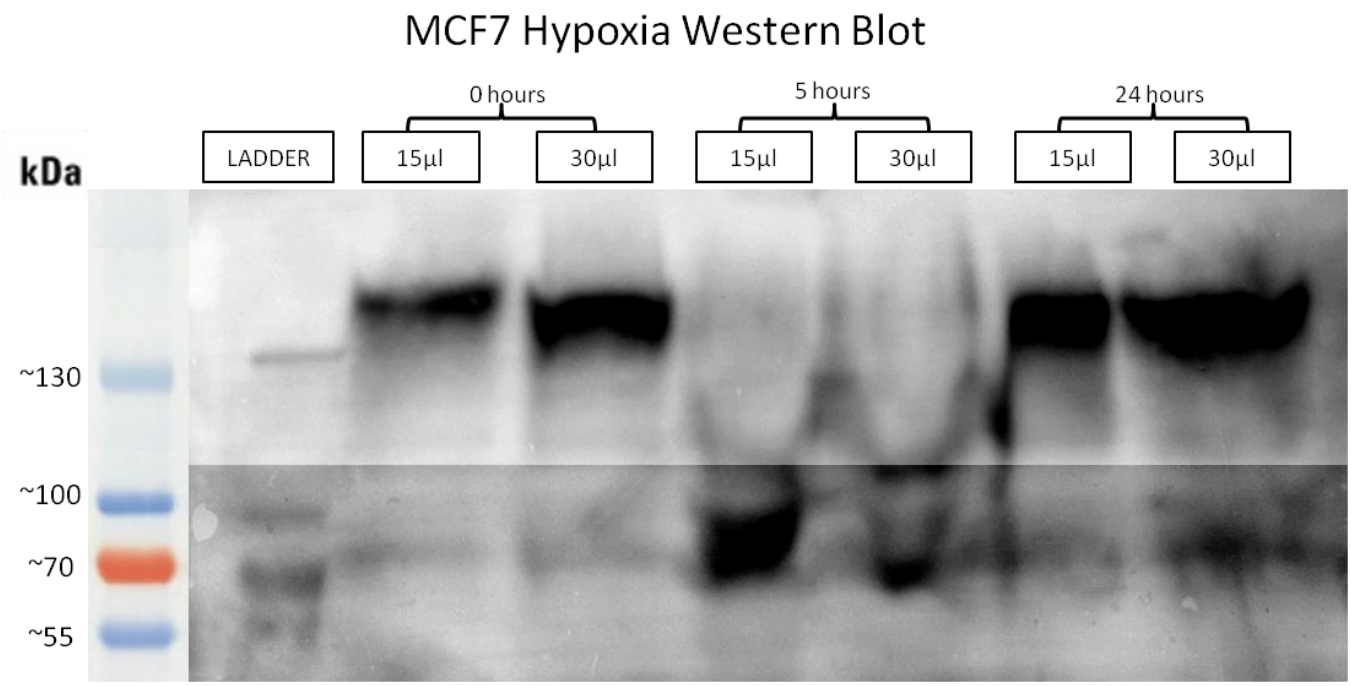

Figure 19: Western Blot analysis of MCF7 cell lysate from cells exposed to hypoxia for 0 (control), 5 and 24 hours. Two volumes of each of the hypoxic sample were loaded to ensure the presence of a visible band. Full short and long exposure blots are displayed in the supplementary figures.

The ERα band appears on the western at ~85kDa and seems to be more pronounced in the 24 hour samples than the 0 hour samples. Unfortunately, the 5 hour sample is not clear but the dark bands present do appear in line with ~85kDa indicating that it is potentially ERα showing up. The intensity of the band is dramatically higher than that seen in 0 or 24 hours but, as with MYOVI the 5 hour time point would need to be repeated.

The western blot suggests that there is a change in expression of MYOVI and ERα induced by hypoxia where there is an upregulation of the production of these proteins within MCF7, this was previously not visible from microscopy (Fig.16) or the mean fluorescence values (Fig.18).

3.2C: Comparison of endogenous MYOVI and ERα/Dab2 distribution in response to hypoxia in MCF7 and HeLa respectively

Comparing the effect of the extrinsic stressor hypoxia between the MCF7 and HeLa cell lines is invaluable in order to infer the pathways in action to allow survival. Figure 21A shows the mean total relative MYOVI fluorescence is higher in MCF7 than in HeLa and while this level remains relatively constant in MCF7 under extending hypoxic condition, HeLa exhibit fluctuating levels of fluorescence with the highest value exhibited at 5 hours hypoxia.

Figure 21B allows the nuclear fluorescence of both cell lines to be compared. Both show a a positive correlation of nuclear MYOVI fluorescence with increasing time under hypoxic conditions, however the levels seen in MCF7 are higher than that seen in HeLa. This is especially prominent after 5 hours of hypoxia where the nuclear fluorescence of MYOVI is double that of HeLa in MCF7.

Most striking is the change in phenotype of both cell lines upon increasing exposure to hypoxia. HeLa morph into filamentous cells and lose adhesion abilities resulting in cells being largely spaced apart and mass cell death is seen. MCF7 however exhibit very little cell death and tend to clump into masses. Examples of this can be seen in the hoescht stained images in Figure 20 and were seen in three separate experiments in 70% of the cells fixed to each slide.

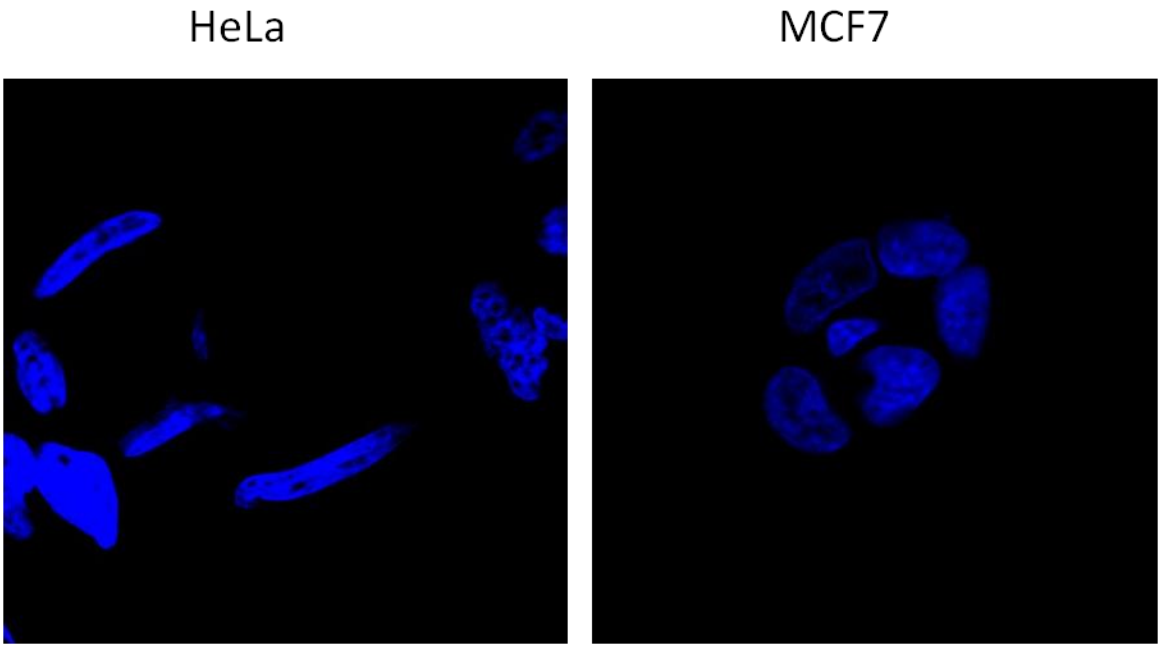

Figure 20: Hoechst only staining of HeLa and MCF7 nuclei after 24 hour exposure to hypoxia.

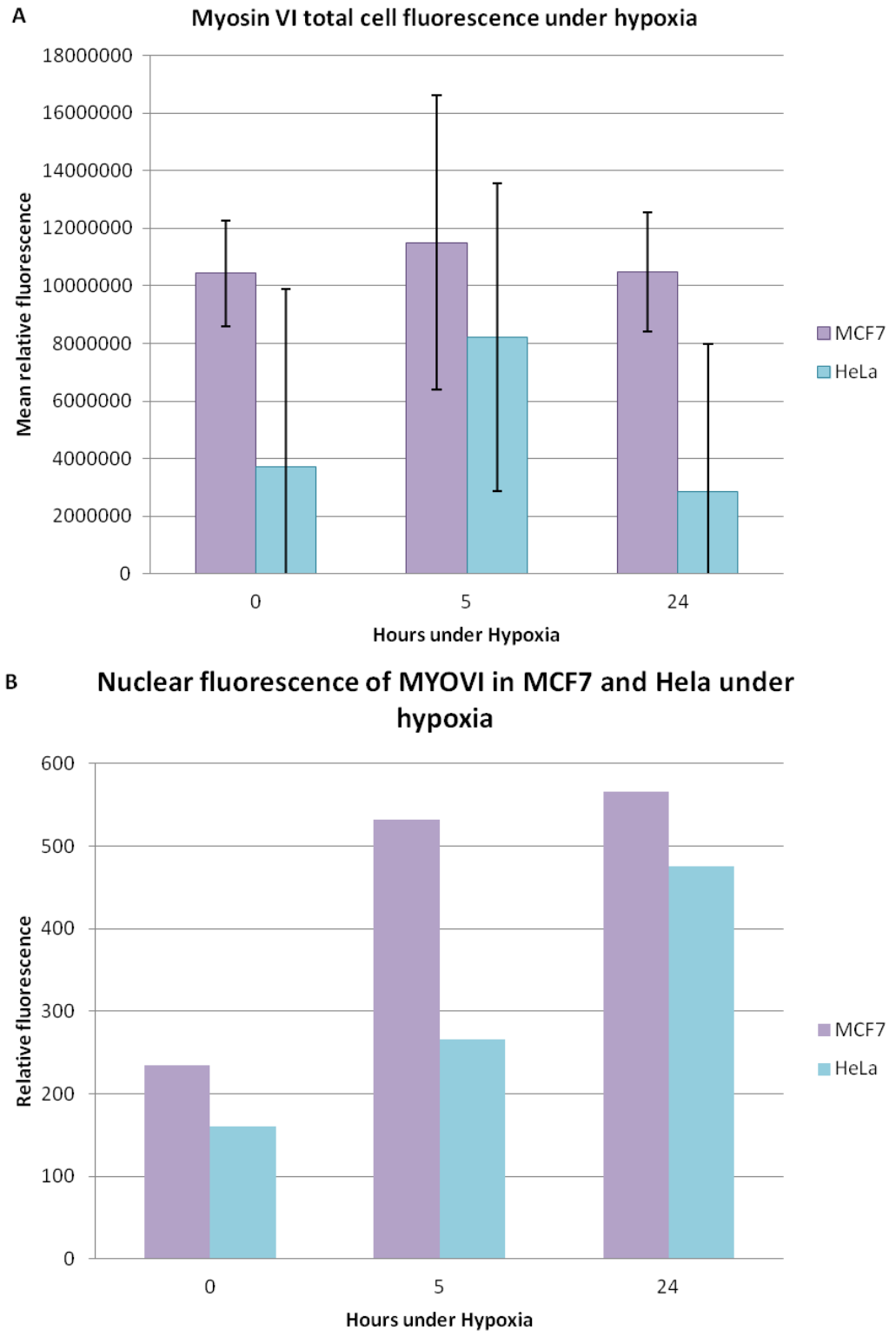

Figure 21: A- A Bar graph showing MYOVI total cell fluorescence in MCF7 and HeLa in 0, 5 and 24 hour hypoxic states. Standard deviation was calculated from raw data collected from 3 single cell microscopy images from different slides for all the conditions. B- A Bar graph displaying the variance in nuclear fluorescence of MYOVI in both MCF7 and HeLa during increasing time under hypoxia. Three nuclei were examined for each condition.

4.0: Summary and Discussion

4.1: Assessing the effect of the ESR1-DAB2 fusion as an intrinsic stressor in MCF7 and HeLa

The ESR1-DAB2 fusion has lost ERα and Dab2 antibody binding epitopes

The primary aim of any transfection is to ensure that the expression of the resultant intrinsic protein can be detected. Typically, this is through a GFP tag introduced to the plasmid which allows instant recognition of a successful transfection using microscopy as cells fluoresce green if they express the introduced protein. In the case of ESR1-DAB2 detection has not been as simple.

The nature of the resultant fusion led to the secondary antibody signal being too weak to differentiate transfected cells from those expressing background fluorescence when imaged with the confocal. This indicated that the primary DAB2 and ERα antibodies were unable to successfully bind to the fusion protein. This could be due to deletion of the recognized epitope by the introduction of DAB2 in the middle of ESR1, or as a result of internalization of the complimentary epitopes, therefore sterically hindering the binding of primary antibodies after tertiary folding and protein maturation (Supplementary Material Fig.1). The plasmid does in fact have an-RFP type fluorophore attached to allow direct detection within cells; however this tag (Rudolph RFP) possesses an odd emission spectra and fluorescence properties that were not viable to image using the microscopes available(Supplementary material- Fig.2). The final option therefore was to utilize the HA tag and acquire a primary antibody that would allow this to be imaged. Ideally this would only detect the ESR1-DAB2 fusion, but as seen in section 3.1, both control samples in HeLa and MCF7 express some level of background non-specific binding of this HA antibody. Nevertheless, this allows the control fluorescence to be compared to that seen in the ESR1-DAB2 transfected samples to confirm a successful transfection.

Transfections were performed using two methods which involved very different delivery of the plasmid into the nucleus of the cell. In previous work re-introducing DAB2 into MCF7, lipofectamine was often too toxic and transfections were unsuccessful where positive results were only obtained from electroporation transfections. In regards to MYOVI expression and localization, the two methods of transfection allowed for a comparison and quantification of nuclear and cytoplasmic populations of the protein in both control and transfected samples.

Both methods of transfection were successful in introducing the ESR1-DAB2 plasmid in both cell lines as seen in the increase in the mean total cell fluorescence of HA increasing throughout. However, as expected lipofectamine induces a wider range of fluorescence in both cell lines indicating that individual cells do not reflect the same expression pattern observed within the population.

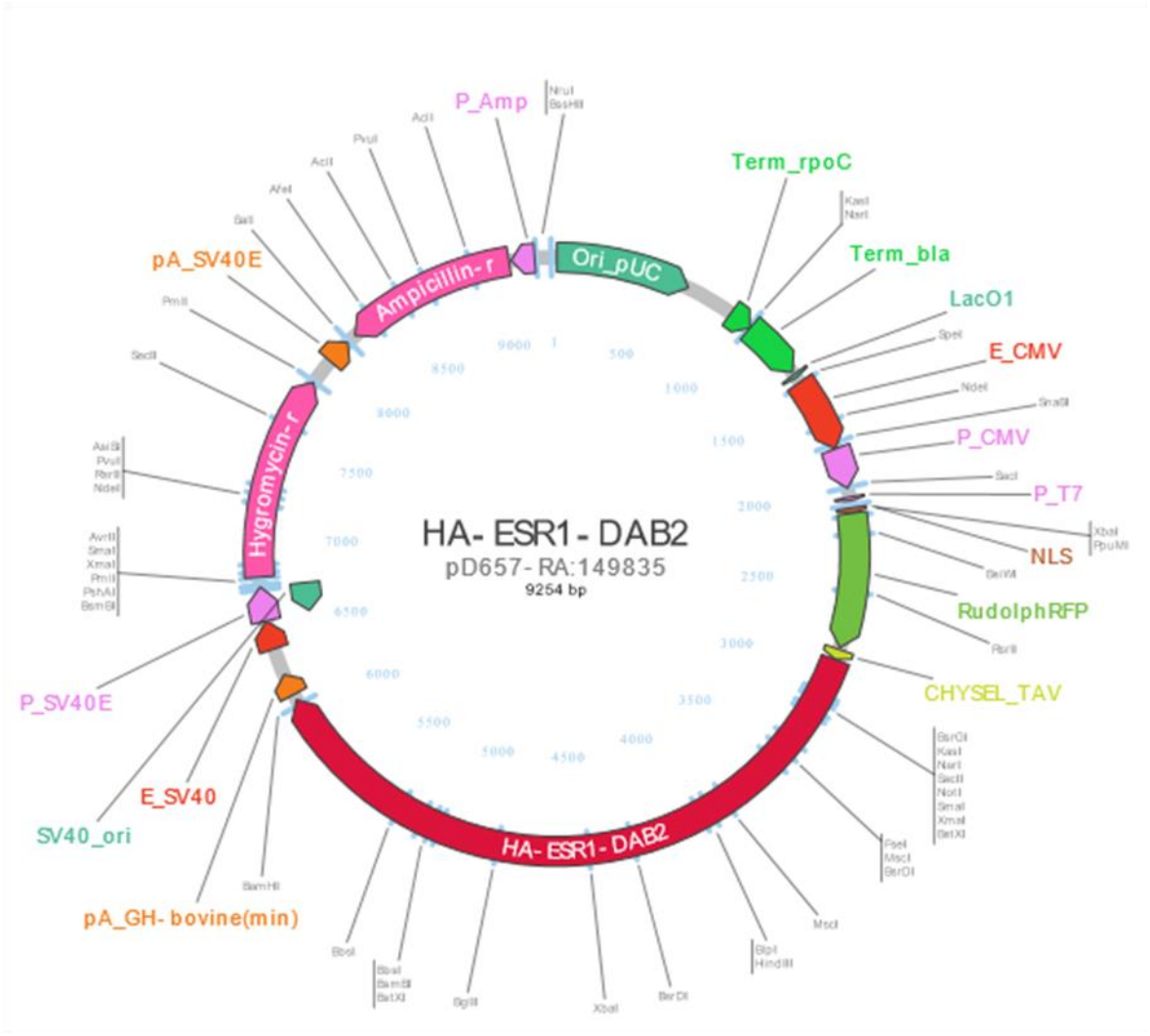

Figure 22: Breakdown Diagram of ESR1-DAB2 fusion plasmid produced by the University of Pittsburg Cancer institute.

In respect to the function of *ESR1-DAB2* within the cancer field, it is integral to examine the function of this fusion within cells and the variation in function depending on the localization of this protein. This novel gene's function has not been explored post-isolation from a metastatic breast cancer patient resistant to therapy. Therefore in vitro studies of its effect on cellular functions within a cervical cancer cell line and breast cancer cell line are invaluable in collecting evidence to suggest signaling pathways that it acts on resulting in this aggressive cancerous phenotype. From a clinical perspective, this could allow for the production and trial of combinatory treatment or a new drug altogether to treat these patients who have no current options. HeLa do not express the ESR1 hormone receptor endogenously, allowing the introduction of ER to be evaluated in respect to its action in altering the protein population and expressed gene profile of these cells and compared to the hormone receptor positive MCF7 cell line.

ESR1-DAB2 localizes within the nucleus in HeLa

Within the cytoplasm PKA, PAK1, Akt and MAPK can act on ERα allowing its phosphorylation(41). This is integral for hormone independent activation within HeLa, as they do not posses hormone receptors like MCF7, instead RTK's on the plasma membrane bind to growth factors and result in the activation of these cytoplasmic kinases which are able to phosphorylate ERα. Hence in both lipofectamine and electroporation transfections, where the HA fluorescence within the nucleus is seen to double, suggest that the ESR1-Dab2 fusion protein is localized within the nuclear compartment. In this case non-phosphorylated ERα can bind to SP-1 and AP-1 resulting in an alternative hormone independent pathway of transcribing target genes; SP-1 targets CG-rich areas within promoter sequences of genes that control cell proliferation and metastasis(42,43) and AP-1 regulates VEGF induced endothelial proliferation (44). Furthermore AP-1 functions to enhance cell invasion via targeting of zinc finger E-box binding homeobox 2 (ZEB2) which downregulates E-cadherin(45).ERα phosphorylated in the cytoplasm further influences transcription of downstream target genes by binding to ERE's in this activated form post migration to the nucleus (46).

However, the fusion protein also contains Dab2, which is endogenously expressed in HeLa and functions as a tumour suppressor. Considering that the expression of ESR1-Dab2 will result in an increase in the levels of functional Dab2 within these cells, there will consequently be an

increase in suppression of Wnt signaling, ERK and TGF-β, pathways associated with metastasis and aggressive cancer phenotypes(47, 48, 49) . DAB2 functionality is exclusively confined to the cytoplasm where it can act on proteins involved in these signaling pathways. ERK1/2 functions within the cytoplasm of cells to activate AP-1 and cyclin-D within the nucleus which lead to cell cycle progression, cell survival, proliferation and angiogenesis (50).Wnt upregulates the activation of β-catenin which accumulates within the cytoplasm before entering the nucleus and exerting its ability in upregulating cell proliferation(51). The images obtained of HeLa through microscopy shows that in both lipofectamine and electroporation transfections, HA fluorescence is mainly exhibited in the cytoplasm, hence the majority of interactions of the ESR1-Dab2 protein will occur here. I would like to highlight that there is crosstalk between the ERα pathway and Dab2 pathway involving the activation of AP-1. While endogenous Dab2 and cytoplasmic ESR1-Dab2 functions to downregulate nuclear AP-1 activation by suppressing the action of ERK1/2, non-phosphorylated ERα within the nucleus can independently activate AP-1. The nuclear proportion of the ESR1-DAB2 protein, which is seen to be present and doubles from the control to the transfected samples, may be interacting directly with DNA via ERE's and transcription factors, to alter the expression of proteins within HeLa as Dab2 does not exhibit nuclear function.

Introduction of ESR1-Dab2 alters MYOVI distribution and exhibit co-localization

As the introduction of ESR1-DAB2 seems to exhibit tumour suppressive, through the action of DAB2, and enhancing properties it is difficult to determine whether this causes a more malignant phenotype within HeLa. Therefore as increased MYOVI is associated with more aggressive cancer phenotypes(52,53), we can look to its expression and localization in order to reveal more about the effect of this fusion within HeLa.

The mean total cell MYOVI fluorescence remains stable between control and transfected cells using both electroporation and lipofectamine transfection methods. The lack of an increase in fluorescence indicates that introduction of *ESR1-DAB2* does not affect the expression of *MYOVI* within cells. In lipofectamine transfections however the level of nuclear MYOVI decreases upon transfection with *ESR1-DAB2* suggesting that a population of MYOVI exits the nucleus and performs cytoplasmic functions. As a large proportion of the ESR1-DAB2 protein is also located here this suggests that LI MYOVI may be interacting with the fusion via the WWY motif as well

as with endogenous DAB2 (54). The interaction of MYOVI LI with DAB2 results in its specific targetting to lipid membranes where it functions as a homodimeric endocytic motor and clusters transmembrane receptors close to clathrin-coated pits (55). From images acquired through microscopy the HA signal does seem to co-localize more strongly in transfected samples (especially in electroporation) in comparison to the controls. This suggests that the function of DAB2 is predominant over the function of ER within the nucleus on gene expression in repressing the activation of ERK1/2 and the Wnt signaling pathway. Moreover we would expect to see an increase in total MYOVI due to its downstream upregulation by ERα if the ESR1-DAB2 protein was heavily involved in affecting gene transcription within the nucleus (56).

ESR1-Dab2 localizes to nuclear compartment in MCF7

Contrastingly MCF7 have lost the endogenous expression of *DAB2* but retain expression and function of ERα and are therefore a hormone sensitive cell line. In lipofectamine transfections the nuclear fluorescence of HA is seen to increase dramatically suggesting that there is a large population of the fusion protein active within the nucleus. As DAB2's function is limited to the cytoplasm, this enrichment within the nucleus proposes that the ESR1 segment of the fusion is resulting in this localization and hence we must consider its function within the nuclear compartment.

A proportion of endogenous ERα (23%) is able to form homodimers via HBD and DBD domains, stabilized by E2, within the cytoplasm which then enters the nuclear compartment (57), however in the case of the fusion protein; we have collected no evidence to indicate that this is possible or occurring. MCF7 also express HER2 and EGFR on the plasma membrane(58). Activation of the ER signaling pathway can originate at these RTK's which contain one transmembrane α-helical structure. Dimerisation is induced by the binding of a signaling molecule, which results in phosphorylation of the cytosolic proportion of these receptors; ERα binds to the cytosolic segment, following lipidation by caveolin-1, which enables E2 activated ERα to associate with Src, PI3K and G-coupled protein α_i . The resultant activation of RAS, a small protein bound to the plasma membrane via a lipid tail, by GTP causes downstream signaling by activating the MAP-kinase cascade. This acts on PI3K within the cytoplasm, producing active MAPK and mTOR, which phosphorylate ERα within the nucleus (59, 60).

Once achieving nuclear localization ERα can act upon ERE's driving the expression of cyclin D1 and CDK4/6, resulting in passage past the G1 checkpoint (61).

ERα has been found to maintain multiple estrogen (E2) dependent interactions within the nucleus, requiring the prior phosphorylation of ERα. One such interaction with cytoplasmic gene regulatory protein STAT, after phosphorylation by PI3K and resultant migration to the nucleus, can directly bind to active chromatin and up-regulate the expression of genes associated with proliferation and survival (62). AP-1 can also be activated via this hormone dependent pathway where ERα in addition to Fos and Jun form a complex to bind DNA. These interactions result in targeting upregulation of genes involved in cell survival, proliferation and metastasis while down-regulating expression of caretaker genes. Such qualities are associated with more aggressive cancer phenotypes and hence indicate that the introduction of ESR1-DAB2 and its presence within the nucleus may be enhancing the endogenous ERα signaling capabilities. While this may be the case, we would also expect to see a dramatic increase in nuclear MYOVI, which from the microscopy images is not found to be present.

Conversely in electroporated samples the nuclear level of HA and hence the level of the fusion protein is not altered from the control, indicating that the dramatic increase in total cell HA fluorescence and successful transfection of ESR1-DAB2 is due to a cytoplasmic population of this protein. The total cell MYOVI level is also seen to double but this is not reflected in a doubling of the nuclear fluorescence. Indicating that MYOVI is also enriched within the cytoplasm and hence not co-localizing with RNAPII in transcription factories at active genes.

<u>ESR1-DAB2 has a function within the cytoplasm of MCF7</u>

As the distribution of ESR1-DAB2 in the electroporated sample is mirrored in MCF7 to that in HeLa, the cytoplasmic role must be considered, specifically in order to suggest why there is disparity between the localization and hence function depending on the method of transfection. One possible scenario, bearing in mind that MCF7 already expresses ERα endogenously, is that the protein is confined to the cytoplasm awaiting phosphorylation and activation by E2. Taking into consideration the doubled level of total MYOVI and its enriched presence within the cytoplasm, this could indicate that the Dab2 portion of the fusion is interacting with MYOVI. I will once again mention that there is no endogenous *DAB2* expression in this cell line. This is

specifically important here as DAB2 interacts within the ER ligand dependent signaling pathway by acting as a negative regulator of ERK1/2 signaling (63). ERK1/2 is activated downstream of ERα binding to E2 via MEK1/2 and induces transcriptional changes via cyclin-D and AP-1 within the nucleus. Over activation of this pathway due to an increase in ERα within this hormone responsive cell line could result in Dab2 recruitment to ERK1/2, preventing phosphorylation to its active form due to its saturation within the cytoplasm(64). This would explain the increased cytoplasmic HA fluorescence and the lack of increased nuclear MYOVI. The western also does not show a definitive increase in MYOVI between the samples loaded, suggesting that ERα within the nucleus is not targeting upregulation of MYOVI transcription. Alternatively the lack of increase in MYOVI could be attributed to ERα's direct feedback loop with P53 (65). P53 binds directly and activated MYOVI's promoter region, its nuclear function is repressed by ERα and this could explain the homeostasis maintained in respect to MYOVI expression (66).

Electroporation with ESR1-DAB2 results in nuclear MYOVI structure

The microscopy images revealed another interesting aspect of MYOVI expression within both HeLa and MCF7 electroporated samples. It is clear to see that in both instances MYOVI within the nucleus seems to localize along a linear structure through the centre of the nucleus. Hoechst staining reveals that the cell is not dividing and therefore this pattern of localization is intriguing. There seems to be no co-localization with the HA fluorescence signal in these cases perhaps suggesting that this is an indirect effect or that electroporation results in the formation of F-actin stress fibers within the nucleus which MYOVI punctuates(67).

4.2: Assessing the effect of hypoxia as an extrinsic stressor on MCF7 and HeLa

Due to differences in expressed genes within HeLa and MCF7, it is particularly interesting to observe the differing effects of hypoxia on these cell lines and compare how MYOVI expression and localization is effected as a result of this extrinsic stressor. Hypoxic conditions mimic the tumour microenvironment and hence changes in cell phenotype and protein expression can infer how and why cells in a tumour mass are able to survive without an immediate oxygen source. Hypoxia can induce a metastatic phenotype as well as increasing glycolysis within cancer cells however intermittent hypoxia has been suggested to have therapeutic potential (68). From a clinical perspective, studying this pathway can allow for more aggressive tumour masses to be treated, and can offer some suggestion as to why current therapies used are unsuccessful in hypoxic tumours (69).

MYOVI is enriched in HeLa nuclei after 5 hours exposure to hypoxia

These experiments focused on only the changes in endogenous expression of MYOVI and Dab2 or ERα in HeLa and MCF7 respectively. Microscopy of HeLa indicated that this cell line could only endure smaller exposure to hypoxia, with the majority of cells at 24 hours dying or expressing high stress states. Therefore we will mostly compare the differences between the control sample (0 hours) to the 5 hour hypoxic sample. While there is a large range of variation in fluorescence the mean total fluorescence of MYOVI is seen to double after 5 hours. This is paired with an increase in MYOVI nuclear fluorescence indicating that specifically the NI MYOVI isoform is enriched in the nucleus as a result of hypoxia. The location of a protein is synonymously indicative of the function it is performing; hence this increase in MYOVI within the nucleus suggests that it is interacting in complex with RNAPII which occurs during transcriptional activity (70). This makes sense under hypoxia because the cell will be responding the external stressor and altering its transcriptional activity in order to upregulate the transcription of genes allowing survival. In normoxia HIF-1α is rapidly degraded by the proteasome complex following polyubiquitination and interaction with Von Hippel-Lindau (VHL), a tumour suppressor. This process is regulated by oxygen-dependent prolyl hydroxylase domain (PHD) enzymes which ensure the rapid degradation of HIF-1α (71).

Hypoxia sensing within cells occurs when HIF-1β and HIF-1α combine to form HIF-1 which can translocate and bind to DNA in the nucleus inducing up-regulated expression of genes involved in metabolic adaptation, apoptosis resistance, angiogenesis and metastasis (72). It is clear that this change in expression pattern within HeLa results in a more aggressive phenotype that has been seen to exhibit resistance to treatment such as radiotherapy. HIF-1 functions as a transcription factor allowing cells to survive hypoxic conditions by up-regulating the expression of glycolytic genes. HIF-2α is also suggested to be responsible for the metabolic adaptation seen, hence promoting cell viability (73).

The mean total fluorescence of DAB2 was also seen to increase and from the microscopy images it is predominantly localized in the cytoplasm where it can interact with MYOVI. This interaction allows MYOVI's targeting to lipid membranes and resultant activation to function as an endocytic motor via dimerisation (74). Hypoxia has been seen to induce internalization of receptors and hence this could explain the enrichment of MYOVI in the cytoplasm performing this function (75, 76). Furthermore, increased *MYOVI* expression results in enhanced secretion of VEGF, where transcription is up-regulated as a downstream target of transcription factor HIF-1(77).

<u>High toxicity in HeLa exposed to 24 hour hypoxia</u>

In regards to the toxicity seen at 24 hours hypoxia, which is not seen in MCF7, the main expression difference is the lack of ERα in HeLa (78). The expression of *HIF-1α* is directly controlled by ERα with the *HIF-1* gene containing an ERE, which ERα can bind, hereby up-regulating transcription (79). As HeLa cannot activate this signaling pathway, the levels of HIF-1α will be lower than that in MCF7, hence resulting in the cell death observed as downstream survival targets are not activated in large enough quantities to cope with the hypoxia (80).

<u>24 hour hypoxia results in upregulation of MTA1 ERα repression in MCF7</u>

Within MCF7 the total mean fluorescence of ER was observed to decrease after 24 hours of hypoxia where previously in the control and 5 hour samples the level remained stable. The sustained hypoxia results in the upregulation of MTA1 (81). MTA1 forms a complex with a histone deacetylase (HDAC) (NuRD complex), which not only stabilizes HIF-1α but also represses ERα transactivation within the nucleus(82).It's function extends to the cytoplasm also

where MTA1 binds ERα, preventing its entry into the nucleus to bind to ERE's (83). This explains the decrease in nuclear fluorescence seen in the microscopy images as transcription of ERα is being repressed and any cytosolic ERα internalized upon E2 binding will be immobilized by MTA1.

MYOI is enriched in the nucleus of MCF7 after 5 hour exposure to hypoxia

While the total mean level of MYOVI fluorescence remains stable in MCF7, the nuclear expression is seen to double at 5 hours from the control and then plateau out at 24 hours. This suggests that MYOVI is being recruited to the nucleus in order to enhance RNAPII transcription of the genes up-regulated by hypoxia which ultimately results in cell survival and continued growth (84). Furthermore MYOVI localization within the cytoplasm seems to favor apical membranes at 24 hours hypoxia. Levels of autophagy are seen to be increased in cells exposed to this extracellular stressor(85), hence MYOVI may be functioning in facilitating autophagosome formation via interactions with nuclear dot protein 52 (NDP52) and Traf6 binding protein (T6BP), resulting in its prominent localization at this membrane(86, 87). Furthermore MYOVI is able to form complexes with adhesion proteins E-cadherin and β-catenin which span the plasma membrane and therefore it may be localizing here in support of the literature suggesting MYOVI and hypoxia increase cell motility and metastasis (88). Interestingly the phenotype of MCF7 cells seems to change to favor clustering; this is possibly in order to share a pool of growth factors that these cells are excreting, specifically VEGF that as mentioned has increased secretion under the action of MYOVI.

4.3 Conclusions

From the data presented, I am confident in saying that transfection of *ESR1-DAB2* was successful in both MCF7 and HeLa, where electroporation seemed to be more effective in producing a smaller variance in results either side of the mean fluorescence measured. Using microscopy images to collect quantative data has its limitations as fluorescence ranges between cell lines making direct comparison difficult as well as within an individual cell line. However, without obtaining a HA-positive control sample a western blot could not be performed and the westerns performed alongside confocal microscopy lead us to believe that neither the DAB2 not ERα antibodies were able to detect the fusion.

Intrinsic stress in the HeLa cells and resulted in lower nuclear MYOVI levels in comparison to that elicited by the extrinsic stressor hypoxia. The literature suggests this may be due to NI MYOVI interacting with RNAPII to enhance its transcription activity of preferentially up-regulated genes enabling cell survival and associated with metastasis. In MCF7 specifically MYOVI is seen to clump within the nucleus suggesting that they may be performing a function within a transcription factory where a set of related genes are actively transcribed.

The total level of MYOVI in HeLa induced by the external stressor increases with extended exposure which contrasts to the expression pattern exhibited by ESR1-DAB2 transfection where it is observed to remain at a steady level. Contrastingly MCF7 exhibits the opposite pattern with the extrinsic stressor eliciting no change in total MYOVI but the internal stressor (introduction of ESR1-Dab2) causes an increase in total MYOVI.

Under the action of an extrinsic stressor MYOVI within MCF7 is seen to localize at apical membranes and this is similar to the distribution pattern seen in lipofectamine transfections suggesting that its main function in these states is confined to interactions with membrane proteins and endosomes within the cytoplasm. However, in electroporation transfections MYOVI can be seen to strongly localize along the external nuclear membrane and co-localizes with the ESR1-DAB2 protein, which is not seen in hypoxia with endogenous ERα. This co-localization seems to be more limited in lipofectamine transfections and in HeLa. MYOVI and endogenous DAB2 within HeLa under hypoxia show higher co-localization than that seen to be induced by ESR1-DAB2.

At 5 hours hypoxia MCF7 exhibits significantly higher nuclear MYOVI levels than that seen in HeLa and while the total MYOVI fluorescence is seen to be steady in response to this extrinsic stressor, HeLa's MYOVI levels fluctuate greatly. In both cell lines 5 hours under hypoxia seems to induce a wider range of effects seen in the wide range of fluorescence exhibited suggesting that this is where the majority of expressional protein changes are occurring in response to the extrinsic stressor. In HeLa the cells do not respond fast enough and therefore they exhibit higher apoptosis than that observed in MCF7 who are very efficient in activating downstream signaling to promote survival in low oxygen conditions.

4.4 Future directions and improvements

While many of the initial aims have been fulfilled by the research collected and displayed here it seems that this is simply the tip of the iceberg. The lack of research involving ESR1-Dab2 within the cancer field means that this research has opened up a whole network of questions and hence future directions for additional research. Furthermore, as is common with cell work, there seems to be a large plethora of improvements that can be made in order to create a stronger portfolio of data supporting one hypothesis. In order to achieve successful transfection of ESR1-Dab2 within these cell lines there was a very large and long optimization procedure, as is expected when performing novel work with novel constructs, which significantly impacted the time frame available to obtain results.

In terms of confirming transfection and determining the amount of resultant protein in the cytoplasmic and nuclear fractions of HeLa and MCF7, it would be ideal to be able to perform a western blot, probing for the HA tag. In order to assess the nuclear localization of ESR1-DAB2, nuclear isolation and lysis could be performed, allowing the amount of fusion protein within this cellular fraction to be assessed and compared to the total cell protein levels. Additionally, it would be interesting to assess the fusions function in comparison to endogenous ERα or DAB2 in MCF7 and HeLa respectively. Knockdowns of these endogenous proteins could be performed using miRNA or siRNA, ensuring a reduced level of the expressed protein before transfecting them with ESR1-DAB2.

To evaluate the proposed interaction between ESR1-DAB2 and MYOVI, immunoprecipitation using a MYOVI antibody attached to the beads in the column would allow for a pull down of proteins forming interactions with this unconventional motor protein. The collected proteins can then be run on a gel in order to determine their size and hence identify them. Should ESR1-DAB2 appear, it would be beneficial to quantify this interaction through a protein binding assay, allowing comparison to endogenous DAB2 binding strength.

Expressing and purifying the ESR1-DAB2 protein would allow the structure to be studied by crystallography to observe expression of functional domains and ensure correct folding. This information is transferrable not only to create mutants but also to design a more specific antibody

for IF and western blots, reducing the background fluorescence seen by using HA antibody. Recombinant DNA technology would allow the construction of mutants, the change in localization of these mutants can allow for the functional domains involved in nuclear localization, DNA binding and MYOVI binding to be highlighted.

The nuclear MYOVI structure seen in electroporation samples could also be probed with actin antibodies to determine if this structure is formed by association with this cytoskeletal component.

Hypoxia has been widely studied as it is seen in physiological processes (embryonic development) and a number of pathophysiological conditions such as atherosclerosis, mountain sickness and of course cancer (89). Within the cancer field, the literature documenting it's effects is extensive, and reveals that hypoxia can result in more aggressive phenotypes or be used as a treatment for specific tumours. This means that many future directions from this research are already being studied, nevertheless the complexity of the system and variation between individual cancers means that the opportunity to accrue more knowledge is endless.

In order to see if the apoptic phenotype observed within HeLa exposed to 24 hours hypoxia is due to the lack of ERα signaling and hence reduced upregulation of HIF-1α, a knockdown of endogenous ERα in MCF7 could be performed before exposure to hypoxia. The comparison of the resultant phenotypes could elucidate how strongly the presence of ERα interacts with signaling pathways activated in hypoxia and if it's deficiency in cells causes apoptosis under this external stressor.

Intermittent hypoxia is suggested to be a method of therapy for treating cancerous tumours, therefore it would be interesting to observe the effects of this cycling hypoxia and normoxia on MYOVI levels and distribution to determine if protein expression is returned to that observed in the control or if the expression remains altered.

As resistance to current cancer therapies is observed in patients with ESR1 mutations and hypoxic tumour microenvironments, examining the change in MYOVI alongside gene expression in these experiments when cells are also treated with a drug currently in clinical use (such as tamoxifen) may allow the methods of resistance to be observed. Potential drugs that can

be used in combinatory treatment to preserve the efficacy of treatment can then be highlighted and tested in the same way.

The final suggestion for future research is to combine the introduction of intrinsic and extrinsic stressors. Exposing ESR1-DAB2 expressing cell lines to hypoxia may be more realistic to the microenvironment observed in breast cancer patients with ESR1 mutations. Hence, observing the resultant phenotype and protein expression could allow for the pathways activated to be understood more deeply, allowing us to expose the methods by which they enable metastasis of the primary tumour and a more aggressive phenotype via resistance. This could be done by creating a stable cell line expressing ESR1-DAB2 and comparing the reaction of these cells in hypoxia to HeLa stably expressing ERα and MCF7 stably expressing DAB2. RT-qPCR can be used to detect changes in mRNA transcripts, hereby quantifying which genes are being actively expressed and up-regulated or down-regulated. Furthermore the relationship between MYOVI and genes up-regulated in this condition can be explored using ChIP, revealing if MYOVI alters gene transcription by functioning in a complex to recruit RNAPII to DNA.

Collecting a wider range of data is beneficial to determine exactly what the ESR1-DAB2 protein is doing within a cell and to see if hypoxia could act as a potential treatment for breast cancer patients exhibiting this *ESR1* mutation who have been seen to be resistant to other routes of therapy. Elucidating the signaling pathways involved in these altered stress states will provide invaluable information for progress within the cancer field and may have limitless clinical implications for current and future patients in regards to therapy.

5.0: References

1. Li, M.-M., Nilsen, A., Shi, Y., Fusser, M., Ding, Y.-H., Fu, Y., … Yang, Y.-G. (2013). ALKBH4-dependent demethylation of actin regulates actomyosin dynamics. *Nature Communications*, *4*, 1832–. http://doi.org/10.1038/ncomms2863
2. Hussain, S., Molloy, J. E., & Khan, S. M. (2013). Spatiotemporal Dynamics of Actomyosin Networks. *Biophysical Journal*, *105*(6), 1456–1465. http://doi.org/10.1016/j.bpj.2013.08.001
3. Aguilar-Cuenca, R., Juanes-García, A. & Vicente-Manzanares, M. Cell. Mol. Life Sci. (2014) 71: 479. https://doi.org/10.1007/s00018-013-1439-5
4. Lin, Y., & Zheng, Y. (2015). Approaches of targeting Rho GTPases in cancer drug discovery. *Expert Opinion on Drug Discovery*, *10*(9), 991–1010. http://doi.org/10.1517/17460441.2015.1058775
5. Alan, J. K., & Lundquist, E. A. (2013). Mutationally activated Rho GTPases in cancer. *Small GTPases*, *4*(3), 159–163. http://doi.org/10.4161/sgtp.26530
6. Cancer Research UK, 2017, [ONLINE] available at: http://www.cancerresearchuk.org/about-cancer/breast-cancer/about [accessed 18 June 2018
7. Makhoul, I., Atiq, M., Alwbari, A., & Kieber-Emmons, T. (2018). Breast Cancer Immunotherapy: An Update. *Breast Cancer : Basic and Clinical Research*, *12*, 1178223418774802. http://doi.org/10.1177/1178223418774802
8. Takeshita, T., Yamamoto, Y., Yamamoto-Ibusuki, M., Tomiguchi, M., Sueta, A., Murakami, K., … Iwase, H. (2017). Comparison of *ESR1* Mutations in Tumor Tissue and Matched Plasma Samples from Metastatic Breast Cancer Patients. *Translational Oncology*, *10*(5), 766–771. http://doi.org/10.1016/j.tranon.2017.07.004
9. Buss, F., Spudich, G., Kendrick-Jones, J., (2004), MYOSIN VI: Cellular Functions and Motor Properties, Annual Review of Cell and Developmental Biology 20:1, 649-676
10. Spudich, J.A. & Sivaramakrishnan, S., (2010) Myosin VI: an innovative motor that challenged the swinging lever arm hypothesis, Nature Reviews, Molecular Cell Biology, vol 11, pg 128–137, DOI 10.1038/nrm2833

11. G. Spudich, M.V. Chibalina, J. Sui-Yan Au, S.D. Arden, F. Buss, J. Kendrick-Jones, Myosin VI targeting to clathrin-coated structures and dimerisation is mediated by binding to Disabled-2 and PtdIns, Nat Cell Biol. 2007 February ; 9(2): pg 176–183
12. Vreugde, S., Ferrai, Miluzio, A., Hauben, E., Marchisio, P.C., Crippa, M.P., Bussi, M., Biffo, S., (2006) Nuclear Myosin VI Enhances RNA Polymerase II-Dependent Transcription, Molecular Cell 23, 749–755, DOI 10.1016/j.molcel.2006.07.005
13. Sayeed, A., Konduri, S.D, Liu, W., Bansal, S., Li, F., Das, G.M., (2007), Estrogen Receptor α Inhibits p53-Mediated Transcriptional Repression: Implications for the Regulation of Apoptosis, Cancer Res, 67(16) 7746-7755; **DOI:** 10.1158/0008-5472.CAN-06-3724
14. You, W., Tan, G., Sheng, N., Gong, J., Yan, J., Chen, D., … Wang, Z. (2016). Downregulation of myosin VI reduced cell growth and increased apoptosis in human colorectal cancer. *Acta Biochimica et Biophysica Sinica*, *48*(5), 430–436. http://doi.org/10.1093/abbs/gmw020)
15. Bond, L. M., Arden, S. D., Kendrick-Jones, J., Buss, F., & Sellers, J. R. (2012). Dynamic Exchange of Myosin VI on Endocytic Structures. *The Journal of Biological Chemistry*, *287*(46), 38637–38646. http://doi.org/10.1074/jbc.M112.373969
16. Tumbarello, D. A., Kendrick-Jones, J., & Buss, F. (2013). Myosin VI and its cargo adaptors – linking endocytosis and autophagy. *Journal of Cell Science*, *126*(12), 2561–2570. http://doi.org/10.1242/jcs.095554
17. Liu, L., Xu, C., Hsieh, J.-T., Gong, J., & Xie, D. (2016). DAB2IP in cancer. *Oncotarget*, *7*(4), 3766–3776. http://doi.org/10.18632/oncotarget.6501
18. Zhang, Z., Chen, Y., Tang, J., & Xie, X. (2014). Frequent Loss Expression of *Dab2* and Promotor Hypermethylation in Human Cancers: A Meta-Analysis and Systematic Review. *Pakistan Journal of Medical Sciences*, *30*(2), 432–437
19. Lee, H.-R., Kim, T.-H., & Choi, K.-C. (2012). Functions and physiological roles of two types of estrogen receptors, ERα and ERβ, identified by estrogen receptor knockout mouse. *Laboratory Animal Research*, *28*(2), 71–76. http://doi.org/10.5625/lar.2012.28.2.71

20. Jeselsohn, R., Buchwalter, G., De Angelis, C., Brown, M., & Schiff, R. (2015). *ESR1* mutations as a mechanism for acquired endocrine resistance in breast cancer. *Nature Reviews. Clinical Oncology*, *12*(10), 573–583. http://doi.org/10.1038/nrclinonc.2015.117
21. Miyamoto, T., Tanikawa, C., Yodsurang, V., Zhang, Y.-Z., Imoto, S., Yamaguchi, R., … Matsuda, K. (2017). Identification of a p53-repressed gene module in breast cancer cells. *Oncotarget*, *8*(34), 55821–55836. http://doi.org/10.18632/oncotarget.19608
22. . Lin, C.-Y., Ström, A., Vega, V. B., Li Kong, S., Li Yeo, A., Thomsen, J. S., … Liu, E. T. (2004). Discovery of estrogen receptor α target genes and response elements in breast tumor cells. *Genome Biology*, *5*(9), R66. http://doi.org/10.1186/gb-2004-5-9-r66
23. Giretti, M. S., Fu, X.-D., De Rosa, G., Sarotto, I., Baldacci, C., Garibaldi, S., … Simoncini, T. (2008). Extra-Nuclear Signalling of Estrogen Receptor to Breast Cancer Cytoskeletal Remodelling, Migration and Invasion. *PLoS ONE*, *3*(5), e2238. http://doi.org/10.1371/journal.pone.0002238
24. Zheng, S., Huang, J., Zhou, K., Zhang, C., Xiang, Q., Tan, Z., … Fu, X. (2011). 17β-Estradiol Enhances Breast Cancer Cell Motility and Invasion via Extra-Nuclear Activation of Actin-Binding Protein Ezrin. *PLoS ONE*, *6*(7), e22439. http://doi.org/10.1371/journal.pone.0022439
25. Tao Z, Shi A, Lu C, Song T, Zhang Z, Zhao J. Breast Cancer: Epidemiology and Etiology. Cell Biochem Biophys. 2015;72(2):333–8
26. Ma C.X., Reinert T., Chmielewska I., Ellis M.J., (2015) Mechanisms of aromatase inhibitor resistance. Nat Rev Cancer, 15(5):261–75, doi: 10.1038/nrc3920
27. Roy, S., & Vadlamudi, R. K. (2012). Role of Estrogen Receptor Signaling in Breast Cancer Metastasis. *International Journal of Breast Cancer*, *2012*, 654698. http://doi.org/10.1155/2012/654698
28. Sen, N., Gui, B., & Kumar, R. (2014). Physiological functions of MTA family of proteins. *Cancer Metastasis Reviews*, *33*(4), 869–877. http://doi.org/10.1007/s10555-014-9514-4
29. Hartmaier, R.J., Puhalla, S.L., Oesterreich, S., Bahreini, A., Davidson, N.E., Brufsky, A.M., Lee, A.V, (2014) Identification of base pair mutations and structural rearrangements acquired in breast cancer metastases including a novel hyperactive ESR1-DAB2 fusion gene specifically in hormone-resistant recurrence [abstract]. In:

Proceedings of the Thirty-Seventh Annual CTRC-AACR San Antonio Breast Cancer Symposium: Dec 9-13; San Antonio, TX. Philadelphia (PA): AACR; Cancer Res 2015;75(9 Suppl):Abstract nr S1-03

30. Bishop, A. J. R., & Schiestl, R. H. (2002). Homologous Recombination and Its Role in Carcinogenesis. *Journal of Biomedicine and Biotechnology*, *2*(2), 75–85. http://doi.org/10.1155/S1110724302204052
31. Yao, Y., & Dai, W. (2014). Genomic Instability and Cancer. *Journal of Carcinogenesis & Mutagenesis*, *5*, 1000165. http://doi.org/10.4172/2157-2518.1000165
32. Muz, B., de la Puente, P., Azab, F., & Azab, A. K. (2015). The role of hypoxia in cancer progression, angiogenesis, metastasis, and resistance to therapy. *Hypoxia*, *3*, 83–92. http://doi.org/10.2147/HP.S93413
33. Rofstad EK, Gaustad JV, Egeland TA, Mathiesen B, Galappathi K. Tumors exposed to acute cyclic hypoxic stress show enhanced angiogenesis, perfusion and metastatic dissemination. Int J Cancer. 2010;127(7):1535–1546
34. Pires, I. M., Bencokova, Z., Milani, M., Folkes, L. K., Li, J.-L., Stratford, M. R., … Hammond, E. M. (2010). Effects of acute versus chronic hypoxia on DNA damage responses and genomic instability. *Cancer Research*, *70*(3), 925–935. http://doi.org/10.1158/0008-5472.CAN-09-2715
35. Luoto, K. R., Kumareswaran, R., & Bristow, R. G. (2013). Tumor hypoxia as a driving force in genetic instability. *Genome Integrity*, *4*, 5. http://doi.org/10.1186/2041-9414-4-5
36. Shah, T., Krishnamachary, B., Wildes, F., Mironchik, Y., Kakkad, S. M., Jacob, D., … Bhujwalla, Z. M. (2015). HIF isoforms have divergent effects on invasion, metastasis, metabolism and formation of lipid droplets. *Oncotarget*, *6*(29), 28104–28119.
37. Ziello, J. E., Jovin, I. S., & Huang, Y. (2007). Hypoxia-Inducible Factor (HIF)-1 Regulatory Pathway and its Potential for Therapeutic Intervention in Malignancy and Ischemia. *The Yale Journal of Biology and Medicine*, *80*(2), 51–60.
38. Zhang, M., Gao, C.-E., Chen, W.-L., Tang, Y.-Y., Nie, J.-Y., Shen, L.-D., … Chen, D.-D. (2018). Opposite response to hypoxia by breast cancer cells between cell proliferation and cell migration: A clue from microRNA expression profile. *Oncology Letters*, *15*(3), 2771–2780. http://doi.org/10.3892/ol.2017.7636

39. Lee, A.V., Oesterreich, S., Davidson, N.E., (2015) MCF-7 Cells—Changing the Course of Breast Cancer Research and Care for 45 Years, *JNCI: Journal of the National Cancer Institute*, Volume 107, Issue 7, https://doi.org/10.1093/jnci/djv073
40. Ambros, P.F. & Karlic, H.I. Hum Genet (1987) 77: 251. https://doi.org/10.1007/BF00284479
41. Arnal, J.F, Lenfant, F., Metivier, R., Flouriot, G. Et al. (2017). Membrane and Nuclear Estrogen Receptor alpha actions: from tissue specificity to medical implications, Physiol Rev. 97(3):1045-1087. doi: 10.1152/physrev.00024.2016.
42. Li, L., Davie, J.R., (2010). The role of Sp1 and Sp3 in normal and cancer cell biology, Annals of Anatomy - Anatomischer Anzeiger, Volume 192(5), 275-283, ISSN 0940-9602, https://doi.org/10.1016/j.aanat.2010.07.010
43. Vizcaíno,C., Mansilla, S., Portugal, J., (2015). Sp1 transcription factor: A long-standing target in cancer chemotherapy, Pharmacology & Therapeutics, Volume 152, 111-124, ISSN 0163-7258, https://doi.org/10.1016/j.pharmthera.2015.05.008
44. Jia, J., Ye, T., Cui, P., Hua, Q., Zeng, H., & Zhao, D. (2016). AP-1 transcription factor mediates VEGF-induced endothelial cell migration and proliferation. *Microvascular Research*, *105*, 103–108. http://doi.org/10.1016/j.mvr.2016.02.004
45. Zhao, C., Qiao, Y., Jonsson, P., Wang, J., Xu, L., Rouhi, P., Sinha, I., Cao, Y., Williams, C., Wright, K.D., (2014). Genome-wide Profiling of AP-1–Regulated Transcription Provides Insights into the Invasiveness of Triple-Negative Breast Cancer, vol. 74(14), DOI: 10.1158/0008-5472.CAN-13-
46. Oleaga, C., Welten, S., Belloc, A., Rodriguez, L., Sole, A., et al. (2012). Identification of novel Sp1 targets involved in proliferation and cancer by functional genomics, Biomedical pharmacology, vol. 84(12), 1581-1591. https://doi.org/10.1016/j.bcp.2012.09.014
47. Loh, Y. N., Hedditch, E. L., Baker, L. A., Jary, E., Ward, R. L., & Ford, C. E. (2013). The Wnt signalling pathway is upregulated in an *in vitro* model of acquired tamoxifen resistant breast cancer. *BMC Cancer*, *13*, 174. http://doi.org/10.1186/1471-2407-13-174
48. Liu, Z., Rebowe, R. E., Wang, Z., Li, Y., Wang, Z., DePaolo, J. S., … Liu, W. (2014). KIF3a Promotes Proliferation and Invasion via Wnt Signaling in Advanced Prostate

Cancer. *Molecular Cancer Research : MCR*, *12*(4), 491–503. http://doi.org/10.1158/1541-7786.MCR-13-0418

49. Cai, J., Guan, H., Fang, L., Yang, Y., Zhu, X., Yuan, J., … Li, M. (2013). MicroRNA-374a activates Wnt/β-catenin signaling to promote breast cancer metastasis. *The Journal of Clinical Investigation*, *123*(2), 566–579. http://doi.org/10.1172/JCI65871
50. Wang, W.-L., Chang, W.-L., Yang, H.-B., Wang, Y.-C., Chang, I.-W., Lee, C.-T., … Sheu, B.-S. (2016). Low disabled-2 expression promotes tumor progression and determines poor survival and high recurrence of esophageal squamous cell carcinoma. *Oncotarget*, *7*(44), 71169–71181. http://doi.org/10.18632/oncotarget.8460
51. Pai, S. G., Carneiro, B. A., Mota, J. M., Costa, R., Leite, C. A., Barroso-Sousa, R., … Giles, F. J. (2017). Wnt/beta-catenin pathway: modulating anticancer immune response. *Journal of Hematology & Oncology*, *10*, 101. http://doi.org/10.1186/s13045-017-0471-6
52. Puri, C., Chibalina, M. V., Arden, S. D., Kruppa, A. J., Kendrick-Jones, J., & Buss, F. (2010). Overexpression of myosin VI in prostate cancer cells enhances PSA and VEGF secretion, but has no effect on endocytosis. *Oncogene*, *29*(2), 188–200. http://doi.org/10.1038/onc.2009.328
53. Polakis, P. (2012). Wnt Signaling in Cancer. *Cold Spring Harbor Perspectives in Biology*, *4*(5), a008052. http://doi.org/10.1101/cshperspect.a008052
54. Dance, A.L., Miller, M., Seragaki, S., Aryal, P., White, B., Aschenbrenner, L., Hasson, T (2004). Regulation of myosin-VI tragetting to endocytic compartments, Traffic.;5(10):798-813. https://doi.org/10.1111/j.1600-0854.2004.00224
55. Bond, L. M., Arden, S. D., Kendrick-Jones, J., Buss, F., & Sellers, J. R. (2012). Dynamic Exchange of Myosin VI on Endocytic Structures. *The Journal of Biological Chemistry*, *287*(46), 38637–38646. http://doi.org/10.1074/jbc.M112.373969
56. Jung, E. J., Liu, G., Zhou, W., & Chen, X. (2006). Myosin VI Is a Mediator of the p53-Dependent Cell Survival Pathway. *Molecular and Cellular Biology*, *26*(6), 2175–2186. http://doi.org/10.1128/MCB.26.6.2175-2186.2006
57. Iwabuchi, E., Miki, Y., Ono, K., Onodera, Y., & Sasano, H. (2017). *In Situ*Evaluation of Estrogen Receptor Dimers in Breast Carcinoma Cells: Visualization of Protein-Protein

Interactions. *Acta Histochemica et Cytochemica*, *50*(2), 85–93. http://doi.org/10.1267/ahc.17011

58. Subik, K., Lee, J.-F., Baxter, L., Strzepek, T., Costello, D., Crowley, P., … Tang, P. (2010). The Expression Patterns of ER, PR, HER2, CK5/6, EGFR, Ki-67 and AR by Immunohistochemical Analysis in Breast Cancer Cell Lines. *Breast Cancer : Basic and Clinical Research*, *4*, 35–41.
59. Barone, I., Brusco, L., & Fuqua, S. A. W. (2010). Estrogen Receptor Mutations and Changes in Downstream Gene Expression and Signaling. *Clinical Cancer Research : An Official Journal of the American Association for Cancer Research*, *16*(10), 2702–2708. http://doi.org/10.1158/1078-0432.CCR-09-175
60. Butti, R., Das, S., Gunasekaran, V. P., Yadav, A. S., Kumar, D., & Kundu, G. C. (2018). Receptor tyrosine kinases (RTKs) in breast cancer: signaling, therapeutic implications and challenges. *Molecular Cancer*, *17*, 34. http://doi.org/10.1186/s12943-018-0797-x
61. Sabbah, M., Courilleau, D., Mester, J., & Redeuilh, G. (1999). Estrogen induction of the cyclin D1 promoter: Involvement of a cAMP response-like element. *Proceedings of the National Academy of Sciences of the United States of America*, *96*(20), 11217–11222.
62. Alvarez, J.V., Frank, D.A., (2004) Genome-wide analysis of STAT target genes: Elucidating the mechanism of STAT-mediated oncogenesis, Cancer Biology & Therapy, 3:11, 1045-1050, DOI: 10.4161/cbt.3.11.1172
63. Lin, J. J., Riely, G. J., & Shaw, A. T. (2017). Targeting ALK: Precision Medicine Takes On Drug Resistance. *Cancer Discovery*, *7*(2), 137–155. http://doi.org/10.1158/2159-8290.CD-16-1123
64. Xu, S., Zhu, J., & Wu, Z. (2014). Loss of Dab2 Expression in Breast Cancer Cells Impairs Their Ability to Deplete TGF-β and Induce Tregs Development via TGF-β. *PLoS ONE*, *9*(3), e91709. http://doi.org/10.1371/journal.pone.0091709
65. Berger, C., Qian, Y., & Chen, X. (2013). The p53-Estrogen Receptor Loop in Cancer. *Current Molecular Medicine*, *13*(8), 1229–1240.
66. Wickramasekera, N. T., & Das, G. M. (2014). Tumor Suppressor p53 and Estrogen Receptors in Nuclear–Mitochondrial Communication. *Mitochondrion*, *0*, 26–37. http://doi.org/10.1016/j.mito.2013.10.002

67. Hendzel, M.J., (2014). The F-act's of nuclear actin, Current opinion in Cell Biology, 28, 84-89, https://doi.org/10.1016/j.ceb.2014.04.003
68. Navarrete-Opazo, A., & Mitchell, G. S. (2014). Therapeutic potential of intermittent hypoxia: a matter of dose. *American Journal of Physiology - Regulatory, Integrative and Comparative Physiology*, *307*(10), R1181–R1197. http://doi.org/10.1152/ajpregu.00208.2014
69. Lu, X., & Kang, Y. (2010). Hypoxia and hypoxia-inducible factors (HIFs): master regulators of metastasis. *Clinical Cancer Research : An Official Journal of the American Association for Cancer Research*, *16*(24), 5928–5935. http://doi.org/10.1158/1078-0432.CCR-10-1360
70. Vreugde, S., Ferrai, C., Miluzio, A., Hauben, E., Marchisio, P.C., Crippa, M.P., Bussi, M., Biffo, S., (2006). Nuclear myosin VI enhances RNA polymerase II-dependent transcription, Mol Cell., 1;23(5):759-55. https://doi.org/10.1016/j.molcel.2006.07.005
71. Forristal, C. E., & Levesque, J.-P. (2014). Targeting the Hypoxia-Sensing Pathway in Clinical Hematology. *Stem Cells Translational Medicine*, *3*(2), 135–140. http://doi.org/10.5966/sctm.2013-0134
72. Bousquet, P. A., Sandvik, J. A., Arntzen, M. Ø., Jeppesen Edin, N. F., Christoffersen, S., Krengel, U., … Thiede, B. (2015). Hypoxia Strongly Affects Mitochondrial Ribosomal Proteins and Translocases, as Shown by Quantitative Proteomics of HeLa Cells. *International Journal of Proteomics*, *2015*, 678527. http://doi.org/10.1155/2015/678527
73. Xiong, J., Zhu, F.F., and Nie, M.F., (2015) Hypoxia-inducible factor-2α (HIF-2α) mediates the effects of hypoxia on the promotion of HeLa cell viability, colony formation, and invasion capacity in vitro, DOI http://dx.doi.org/10.4238/2015.April.13.7
74. Altman, D., Goswami, D., Hasson, T., Spudich, J. A., & Mayor, S. (2007). Precise Positioning of Myosin VI on Endocytic Vesicles In Vivo . *PLoS Biology*, *5*(8), e210. http://doi.org/10.1371/journal.pbio.0050210
75. Xi, C., Liang, X., Chen, C., Babazada, H., Li, T., & Liu, R. (2017). Hypoxia induces Internalization of Kappa Opioid Receptor. *Anesthesiology*, *126*(5), 842–854. http://doi.org/10.1097/ALN.0000000000001571)

76. Coelho, J.E., Rebola, N., Fragata, I., Ribeiro, J.A., de Mendonça, A., Cunha, R.A., (2006) Hypoxia-induced desensitization and internalization of adenosine A1 receptors in the rat hippocampus, Neuroscience, 138(4):1195-203, https://doi.org/10.1016/j.neuroscience.2005.12.012

77. Puri, C., Chibalina, M. V., Arden, S. D., Kruppa, A. J., Kendrick-Jones, J., & Buss, F. (2010). Overexpression of myosin VI in prostate cancer cells enhances PSA and VEGF secretion, but has no effect on endocytosis. *Oncogene*, *29*(2), 188–200. http://doi.org/10.1038/onc.2009.328

78. Huderson, B. P., Duplessis, T. T., Williams, C. C., Seger, H. C., Marsden, C. G., Pouey, K. J., … Rowan, B. G. (2012). Stable Inhibition of Specific Estrogen Receptor α (ERα) Phosphorylation Confers Increased Growth, Migration/Invasion, and Disruption of Estradiol Signaling in MCF-7 Breast Cancer Cells. *Endocrinology*, *153*(9), 4144–4159. http://doi.org/10.1210/en.2011-2001

79. Yang, J., AlTahan, A., Jones, D. T., Buffa, F. M., Bridges, E., Interiano, R. B., … Harris, A. L. (2015). Estrogen receptor-α directly regulates the hypoxia-inducible factor 1 pathway associated with antiestrogen response in breast cancer. *Proceedings of the National Academy of Sciences of the United States of America*, *112*(49), 15172–15177. http://doi.org/10.1073/pnas.1422015112

80. TIAN, X., WANG, W., ZHANG, Q., ZHAO, L., WEI, J., XING, H., … CHEN, G. (2010). Hypoxia-inducible factor-1α enhances the malignant phenotype of multicellular spheroid HeLa cells *in vitro*. *Oncology Letters*, *1*(5), 893–897. http://doi.org/10.3892/ol_00000159

81. Wang, R.-A. (2014). MTA1—a stress response protein: a master regulator of gene expression and cancer cell behavior. *Cancer Metastasis Reviews*, *33*(4), 1001–1009. http://doi.org/10.1007/s10555-014-9525-1

82. Yoo, Y.-G., Kong, G., & Lee, M.-O. (2006). Metastasis-associated protein 1 enhances stability of hypoxia-inducible factor-1α protein by recruiting histone deacetylase 1. *The EMBO Journal*, *25*(6), 1231–1241. http://doi.org/10.1038/sj.emboj.7601025

83. Ma, H., Li, L., Dou, G., Wang, C., Li, J., He, H., … Qi, H. (2017). Z-ligustilide restores tamoxifen sensitivity of ERα negative breast cancer cells by reversing

MTA1/IFI16/HDACs complex mediated epigenetic repression of ERα. *Oncotarget*, *8*(17), 29328–29345. http://doi.org/10.18632/oncotarget.16440

84. Manavathi, B., Singh, K., & Kumar, R. (2007). MTA family of coregulators in nuclear receptor biology and pathology . *Nuclear Receptor Signaling*, *5*, e010. http://doi.org/10.1621/nrs.05010
85. Fili, N., Hari-Gupta, Y., dos Santos, Á., Cook, A., Poland, S., Ameer-Beg, S. M., … Toseland, C. P. (2017). NDP52 activates nuclear myosin VI to enhance RNA polymerase II transcription. *Nature Communications*, *8*, 1871. http://doi.org/10.1038/s41467-017-02050-w
86. Fang, Y., Tan, J. and Zhang, Q. (2015), Signaling pathways and mechanisms of hypoxia-induced autophagy in the animal cells. Cell Biology International, 39: 891–898. doi: 10.1002/cbin.10463)
87. Tumbarello, D. A., Kendrick-Jones, J., & Buss, F. (2013). Myosin VI and its cargo adaptors – linking endocytosis and autophagy. *Journal of Cell Science*, *126*(12), 2561–2570. http://doi.org/10.1242/jcs.095554
88. Chibalina, M., Puri, C., Kendrick-Jones, J., & Buss, F. (2009). Potential roles of myosin VI in cell motility. *Biochemical Society Transactions*, *37*(Pt 5), 966–970. http://doi.org/10.1042/BST0370966
89. Gilany, Kambiz & Mohtaram, Vafakhah. (2010). Hypoxia: a Review. Journal of Paramedical Sciences. 1. ISSN 2008-496X
90. Yuan, J., Narayanan, L., Rockwell, S., Glazer, P.M., (2000), Diminished DNA repair and elevated mutagenesis in mammalian cells exposed to hypoxia and low pH, Cancer Res, 60: 4372-4376
91. Cortés Gutiérrez, E. I., García-Vielma, C., Aguilar-Lemarroy, A., Vallejo-Ruíz, V., Piña-Sánchez, P., Zapata-Benavides, P., & Gosalvez, J. (2017). Expression of the HPV18/E6 oncoprotein induces DNA damage. *European journal of histochemistry : EJH*, *61*(2), 2773. doi:10.4081/ejh.2017.2773
92. Olivier, M., Hollstein, M., & Hainaut, P. (2010). TP53 mutations in human cancers: origins, consequences, and clinical use. *Cold Spring Harbor perspectives in biology*, *2*(1), a001008.

6.0: Supplementary Material

6.1- Figures

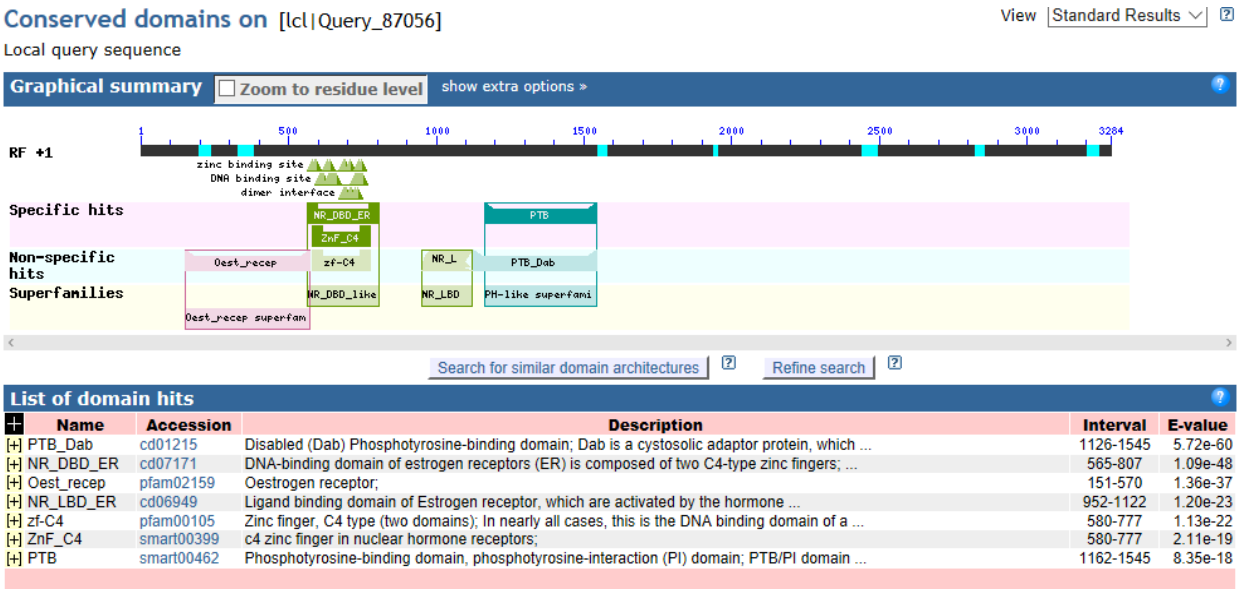

Name	Accession	Description	Interval	E-value
[+] PTB_Dab	cd01215	Disabled (Dab) Phosphotyrosine-binding domain; Dab is a cystosolic adaptor protein, which ...	1126-1545	5.72e-60
[+] NR_DBD_ER	cd07171	DNA-binding domain of estrogen receptors (ER) is composed of two C4-type zinc fingers; ...	565-807	1.09e-48
[+] Oest_recep	pfam02159	Oestrogen receptor;	151-570	1.36e-37
[+] NR_LBD_ER	cd06949	Ligand binding domain of Estrogen receptor, which are activated by the hormone ...	952-1122	1.20e-23
[+] zf-C4	pfam00105	Zinc finger, C4 type (two domains); In nearly all cases, this is the DNA binding domain of a ...	580-777	1.13e-22
[+] ZnF_C4	smart00399	c4 zinc finger in nuclear hormone receptors;	580-777	2.11e-19
[+] PTB	smart00462	Phosphotyrosine-binding domain, phosphotyrosine-interaction (PI) domain; PTB/PI domain ...	1162-1545	8.35e-18

Figure 1: A screenshot of ESR1-Dab2 plasmid sequence screened using basic local alignment search tool (BLAST) created by Uniprot.org.

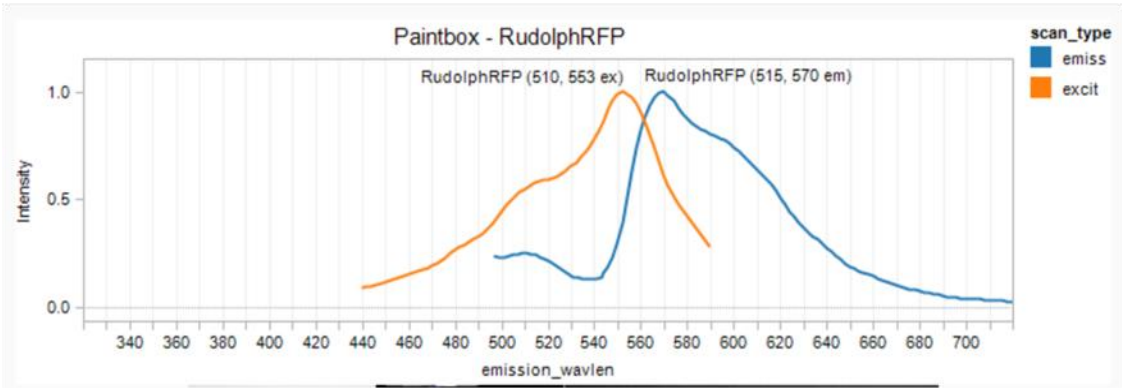

Figure 3: RudolphRFP fluorophore excitation and emission spectra. The fluorophore is created and supplied by ATUM.

A

Primers	Conditions (1/10 cDNA dilution)
B-actin	(1) HeLa control (2) HeLa ESR1-Dab2 fusion (3) MCF7 Control (4) MCF7 ESR1-Dab2 fusion
ERα	
Dab2	

B

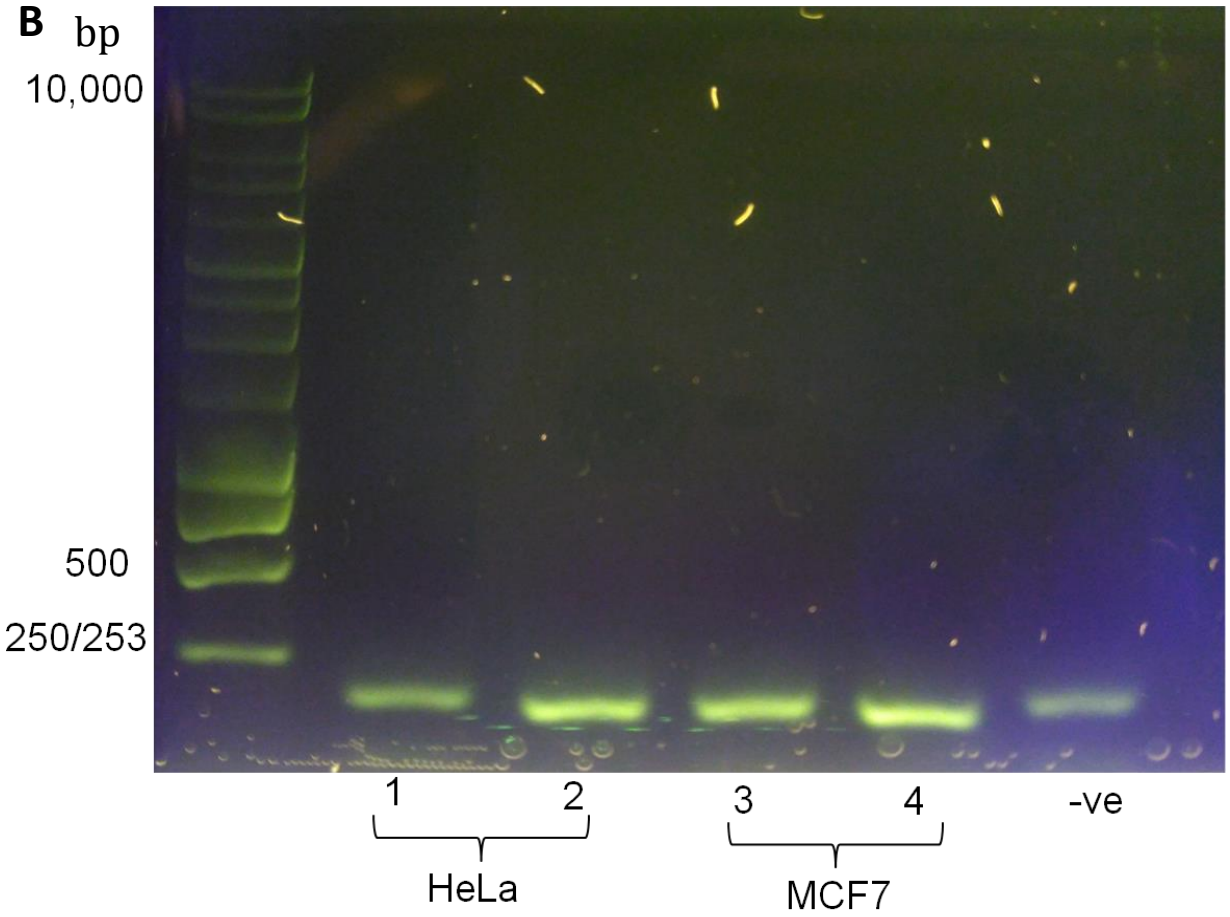

Figure 2: A: A table to display Primers used in PCR techniques and corresponding samples used. Transfection technique used was lipofectamine where RNA was extracted from these cell samples B: Gel of resultant qPCR cDNA products where primer-dimer is the only band present. Samples 1-4 correspond to descriptions defined in the table A and –ve sample is H_2O.

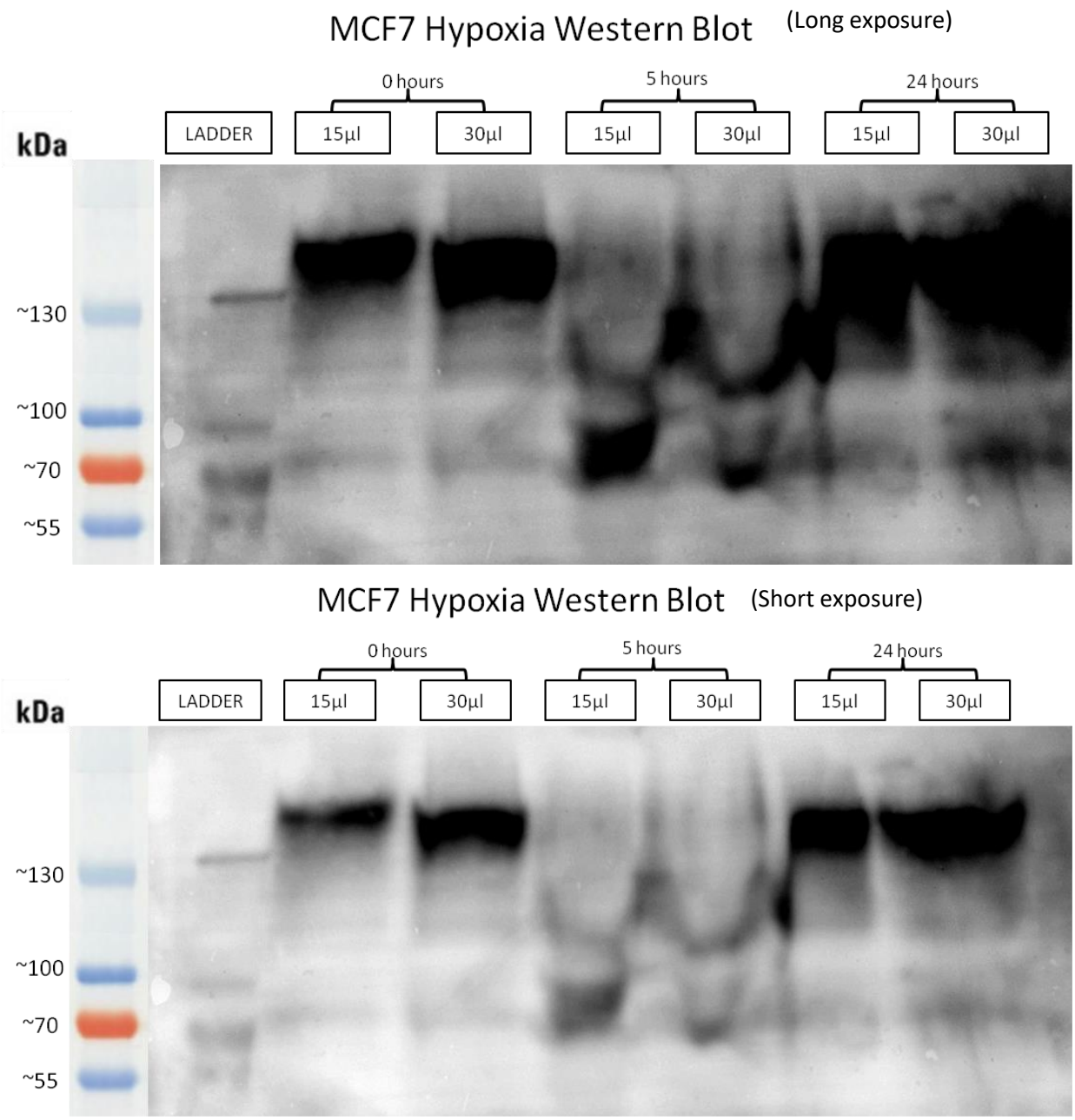

Figure 1: Full images of western blots performed on MCF7 hypoxia samples displaying long and short exposure images.

7.0: Acknowledgments

I would like to thank the members of the Toseland Lad for their support over the course of the last year, specifically Chris Toseland for giving me the opportunity to do a MRes and Yukti Hari-Gupta for training me in cell culture techniques and imaging. Furthermore, Anastasios Tsaousis for the use of the hypoxia hood, Darren Griffin for access to the Olympus BX-61 epifluorescence microscope, Ian Brown, Diego Cantoni, Matthew Badham for training on the confocal microscope and Elliot Piper-Brown, Alia dos Santos for guidance in ImageJ and statistical analysis.